Investigation on the origins of comets as revealed through IR high resolution spectroscopy

I. Molecular abundances

M. Lippi[1,2], G. L. Villanueva[1], M. J. Mumma[1], S. Faggi[1,2]

[1]NASA Goddard Space Flight Center, Solar System Exploration Division, 8800 Greenbelt Rd., Greenbelt, MD, 20771, USA

[2]American University, Dept. of Physics, 4400 Massachusetts Ave NW, Washington DC, 20016, USA

Abstract

We report and analyze molecular abundances updated in twenty comets by employing modern data reduction procedures and molecular models. Using boxplots and scatter plots, we examine how the different molecular species are distributed among the comet population, while by means of pie charts we investigate the relative proportions of these molecular species in each comet. We compare these results with the orbital parameters of the selected targets in order to identify trends related to the dynamical history of each comet. In this way, we identify at least three chemical classes based mainly on relative abundances of CO, CH_3OH, CH_4, C_2H_6, HCN and NH_3. The combination of relative abundances and orbital parameters is then compared with chemical models of planetary system formation and may offer an alternative approach to investigate the origin and evolution of the material in cometary nuclei. Our study also confirms the need to add more objects to our sample in order to improve the statistics, especially for hyper-volatiles (i.e. CH_4 and CO) in Jupiter Family comets.

Keywords: Comets: Composition**,** Spectroscopy**,** Infrared observations**,** Origins

1. Introduction

Comets are cryogenically preserved relics from the formation of the Solar System. They accumulated from the dusty and icy material present in the midplane of our protoplanetary disk system, about 4.6 billion years ago. After formation, they were scattered by strong gravitational interactions with the giant forming planets into their current dynamical reservoirs: the Oort Cloud (OC), considered the primary source of long period and dynamically-new comets, and the scattered disk of the Kuiper Belt (KB), the primary source of short period comets. According to current models (Levison & Morbidelli 2003; Gomes et al. 2005), the majority of the objects that formed between 5 and 17 au likely scattered into the OC reservoir, while those that formed in the outer proto-planetary disk (beyond R_h ~ 17 au) entered both the OC and KB reservoirs. Recent models predict also that a significant fraction of OC comets may have been captured from similar reservoirs surrounding other stars in the Sun's birth cluster (Levison et al. 2010). Once in their reservoirs comet nuclei are expected to remain frozen and slightly unaltered during time: investigating their chemical composition and properties may unveil the conditions present during their formation (e.g. temperature gradient, molecular abundances, and amount of UV/X-ray/cosmic-ray penetration in the protoplanetary disk), and reveal important clues on the early

evolution of the Solar System. Moreover, it could disclose which processes may have changed the nucleus composition after its formation (e.g. cosmic rays impacting the outer layer of the nucleus or successive surface warming on repeated passages through the inner solar system).

A powerful technique to sample the organic composition of comets is high-resolution spectroscopy in the infrared spectral region, between 2 and 5 μm, where it is possible to sample emission lines produced by solar-pumped fluorescence of some primary volatiles (i.e. molecules released directly from the nucleus), such as H_2O, CH_4, C_2H_6, C_2H_2, HCN, NH_3, CH_3OH, H_2CO, and CO. Using this technique it is possible to research three main parameters that are considered cosmogonic: 1) the chemical composition of the nucleus, that is expected to partially reflect the physics and chemistry of the protoplanetary disk where comets formed, 2) the isotopic fractionation in ices, particularly sensitive to the formation temperature, and 3) the nuclear spin statistics (ortho-para-meta, etc.), also sensitive to the formation temperature, and possibly unaltered in time.

Active comets have been studied using high resolution spectroscopy in the infrared since 1985 (Mumma et al. 1986), and the statistical analysis of primary volatiles has revealed a significant chemical diversity among these bodies (see recent taxonomic reviews: Mumma & Charnley 2011; Dello Russo et al. 2016; Bockelée-Morvan & Biver 2017). In Lippi et al. 2020, we demonstrated that some previously reported infrared results may need revisiting due to incomplete molecular models used to interpret the fluorescence emissions, to non-sufficiently accurate atmospheric transmittances, and to small issues in the data analysis extraction methods. Comets that were observed and analyzed before 2011, when novel analysis approaches started to be introduced, are the most impacted, and the re-analysis of their spectra is necessary to identify and remove these biases before applying a reliable statistical analysis.

In this paper we report updated molecular abundances (i.e. Mixing Ratios – MRs, % with respect to water) retrieved in 20 comets using the latest version of data reduction procedures and molecular models available in our team. We investigate the chemical diversity observed among these comets using a descriptive statistical approach, in order to group similar objects and to identify trends among the analyzed molecular species. Finally, we compare our results with recent proto-planetary disk models and try to correlate our abundances with those that are expected in different regions of the disk midplane during the formation and evolution of the Solar System.

2. Data reduction

The 20 comets were selected from our rich database (see Lippi et al. 2020), considering observations performed with the NIRSPEC spectrometer situated at the W. M. Keck Observatory atop Maunakea in Hawaii (McLean et al. 1998). The targets[1], listed in Table 1 together with their observing logs and orbital parameters, were chosen pondering the most sensitive datasets.

[1] From now on we will use the following acronyms to identify the analyzed comets: **07N3**: C/2007 N3 (Lulin); **99S4**: C/1999 S4 (LINEAR); **99H1**: C/1999 H1 (Lee); **09P1**: C/2009 P1 (Garradd); **12S1**: C/2012 S1 (ISON); **12F6**: C/2012 F6 (Lemmon); **99T1**: C/1999 T1 (McNaught); **00WM1**: C/2000 WM1 (LINEAR); **13R1**: C/2013 R1 (Lovejoy); **01A2**: C/2001 A2 (LINEAR); **04Q2**: C/2004 Q2 (Machholz); **07W1**: C/2007 W1 (Boattini); **8P**: 8P/Tuttle; **103P**: 103P/Hartley 2; **73PB**: 73P/Schwassmann–Wachmann (B); **73PC**: 73P/Schwassmann–Wachmann (C); **17P**: 17P/Holmes ; **10P**: 10P/Tempel 2; **9P**: 9P/Tempel 1; **2P**: 2P/Encke

We re-analyzed each dataset in a systematic way using semi-automated tools that improve processing speed and minimize possible human errors. Spectral calibration and compensation for telluric absorption was achieved by comparing the data with highly accurate atmospheric radiance and transmittance models obtained with PUMAS/PSG (Villanueva et al. 2018). Flux calibration was obtained using the spectra of a standard star observed closely in time with the comet, and now reduced with the same current algorithms.

Rotational temperatures and production rates were obtained following the methodology introduced in our previous work (Lippi et al. 2020). Re-analyzed values of nucleus-centered production rates, rotational temperatures, growth factors, and global production rates are presented in the on-line material. For the analysis reported in this paper, in case of non-detections we make use of 2σ upper limits (corresponding to the 95% confidence limit), that we consider significant only if smaller than the median value obtained from the corresponding box plot statistics (see Section 3.1).

Hereafter, we will refer always to mixing ratios with respect to water. If a species is detected during more observing nights, the final MRs reported in Table 2 are calculated as the weighted mean of each single retrieved MR; when we have both detections and 2σ upper limits, the latter are not included in this calculation. When instead in a comet we measure only upper limits, we assume as representative the lowest of these values. Variations in mixing ratios measured in the same comet are usually within 1σ of their respective mean values, and in case of higher dissimilarities, the weighted mean should ensure that the best data dominates.

There is evidence in some comets of possible outgassing variability at different heliocentric distances that can influence to some extent the resulting mixing ratios with respect to water (see for example Mumma et al. 2011; Faggi et al. 2019); also, comets observed farther than 1.5 au from the Sun, may have a small tendency to show higher abundances of hyper-volatiles with respect to other molecules (see for example Gicquel et al. 2015); comets with perihelion distance beyond 2 au show strong effects of this kind (e.g. C/2006 W3 Christensen, Bonev et al. 2017). The relationships between our measured mixing ratios (with respect to water and normalized to their median) and the heliocentric distances at the time of observations is shown in Figure 1: in general, we don't observe these effects, even if a certain trend seems to exist for CO. Most of our targets were observed between about 0.8 and 1.5 au where water is fully active[2], and we don't expect a strong influence of the heliocentric distance on our results. Considering our small sample and the limited orbital range for each analyzed comet, we are not able to determine if an evolution of the outgassing occurred along the orbit, or if the measured values are completely independent from the heliocentric distances. In the following analyses, we will assume the retrieved values to be representative of the nuclear original abundances. Yet, we underly the need for additional statistics, that comprise alternative abundance ratios (e.g. MRs calculated with respect to ethane) and more observing dates for each target in order to analyze if and how the MRs vary with the heliocentric distance; these analyses will be given elsewhere.

[2] Exceptions are only comet 12F6 observed at 1.74 au and 17P observed at about 2.5 au (outburst).

3. Data analysis and discussion

3.1 Box plot statistics and correlation analysis to explore the distribution of molecular species among the comet population

We investigated the distribution of molecular species among the comet population making use of box plots, as shown in Figure 2 (absolute values in panel A, values normalized to the median in panel B). For each molecule, the box plot ranges are calculated using the weighted averaged MRs, that are graphed as filled circles on the right of each box; we didn't include either the measure's uncertainties or 2σ upper limits in the calculation. Upper and lower bounds of each box are fixed at the 75th and 25th percentiles of the distribution, respectively. The whiskers are estimated using the 9th and the 91st percentiles. The boxes are showed in a logarithmic scale, and compared with a gaussian box (the grey box behind the colored one) centered on the median of our measurements and characterized by a standard deviation comparable with the size of the measured box. The box plot statistics are reported in Table 3.

CO and CH_3OH are the molecules that show the highest median values (2.66 and 2.61 respectively) followed by CH_4 (0.78), NH_3 (0.75) and C_2H_6 (0.65). If we consider the Inter Quartile Range Normalized to the median (IQRN), calculated as the difference between the 75th and the 25th percentile bounds, CO is the molecule that presents the highest dispersion (2.39), followed by CH_4 (1.05), H_2CO (0.96), C_2H_6 (0.82), CH_3OH (0.77), C_2H_2 (0.75), NH_3 (0.72), and HCN (0.53).

We calculated the skewness (Skw) of each box distributions as:

$$Skw = \frac{(75^{th}\ percentile - 50^{th}\ percentile)}{(50^{th}\ percentile - 25^{th}\ percentile)}.$$

Almost all analyzed molecular species are described by an upper-skewed (right-skewed, Skw >1) distribution, with the exceptions of C_2H_6 and HCN, that are lower-skewed (left-skewed Skw < 1), and quasi-symmetric with respect to the median. If we assume that the distribution of the studied molecular species should be normally distributed among comets, the separation from the gaussian shape that we observe in our box plots could be a bias related to the small size of our samples. However, an asymmetric box plot could also be indicative of a bi-modal or multi-modal distribution, compatible with distinct chemical populations of comets. Additional data are needed to improve these statistics.

To test the potential effects of the different dynamical histories on the nucleus composition, we investigated the relationships between our mixing ratios and the corresponding Tisserand Invariant (with respect to Jupiter - T_j) as shown in Figure 3. While it is not possible to identify very strong relationships between MRs and T_j in comets, data for C_2H_6, CH_4 and CO display more pronounced dispersions, with OC comets showing higher values than do JF comets, even if exceptions are present (see for example CO in comet 00WM1 or C_2H_6 and CH_4 in comet 99S4). It is important to note that many of the reported MR values for CH_4 and CO in Jupiter family comets consist of 2σ upper limits, so in order to identify clearer trends, many more measurements of these two species in short period comets are necessary.

In Table 4 we report the Spearman's rank-order correlation factor (Sp-Corr) and corresponding statistic: two-sided level of significance (p) and degrees of freedom (n = number of measures-2) for each combination of the studied molecular species. The correlations were calculated using the weighted averaged MRs. Upper limits were not included in these calculations. We have chosen the Spearman's correlation since it corresponds to the non-parametric version of

the Pearson product-moment correlation, and being more general, it assesses how well the relationship between two variables can be described using a monotonic function (not necessarily linear). When the relationship between the two variables is linear, the Spearman's correlation factor should correspond with the Pearson's one. We consider a correlation good when the resulting Spearman's coefficient is Sp-Corr ≥ 0.5 coupled with a level of significance $p \leq 0.05$. If we consider the correlations with degrees of freedom $n \geq 9$ (at least half of the measures used for the calculation of the Spearman's correlation factor), it is possible to notice that the MRs of C_2H_6 are highly correlated with the ones of both CH_4 and C_2H_2 (0.85 and 0.77, respectively), suggesting a potential common origin. The mixing ratios of methanol are highly correlated with MRs of acetylene and ethane (0.74 and 0.82, respectively), and to a lesser extent with those of methane (0.45); it is not clear at the moment why the latter correlation is much lower than the first two. Correlation factors between MRs of CO and hydrocarbons range from 0.45 (for the mixing ratios of C_2H_6) to about 0.7 (for C_2H_2 and CH_4). A negative trend may exist between the relative abundances of HCN and H_2CO (-0.5), while a positive correlation is observed between CH_3OH and H_2CO (0.65). Mixing ratios relative to other molecular species combinations do not show significant correlations or anti-correlations, but it is important to consider that all these relationships may change to an important degree with the addition of new data. As an example, in Figures 4 and 5 we show the relationships of C_2H_6 with CH_3OH, CH_4, and HCN, and the relationship between CO and CH_3OH.

Some of the observed distributions and trends that characterize the molecular species we investigated are tentatively consistent with recent models of proto-planetary disks, where the chemistry is driven mainly by both the temperature gradient and the radiation fields produced by the forming star and the external environment (see for example Walsh et al. 2010; Eistrup et al. 2016, 2018; Bosman et al. 2018; Pontoppidan et al. 2019).

For example, carbon monoxide is expected to be largely gaseous in the inner part of the disk midplane, where temperatures are warmer than its sublimation temperature ($T > 26$ K) and where it will probably react with other molecules and/or radicals to form more complex species, like for example CO_2 (Furuya & Aikawa 2014; Schwarz et al. 2018). At the same time, some preservation mechanisms of interstellar CO can be active when the gas is mixed through the midplane, and at every vertical cycle some of these molecules may freeze-out onto grains and not cycle back to the gas (Kama et al. 2016); this may explain very high abundances of CO in some comets. Conversely, in regions of the disk where the temperatures drop below 26 K, hydrogenation on grain surfaces is thought to become the dominant chemical process, and CO can be efficiently converted to other species, such as CH_3OH (Hiraoka et al. 2005). Being among the most volatile species, CO is also more likely to be lost during the lifetime of a comet, due to heating of the nucleus surface as the comet experiences repeated passages through the inner Solar System, and this is particularly true for Jupiter family comets. All these scenarios are compatible with the large range of MR values that we measure for this molecule, and could suggest that the original information on the CO abundances in some comets may have been lost during time.

Methanol is the least volatile species among the analyzed trace gases, and it shows a less extended distribution compared with CO. Methanol has no known efficient gas-phase formation route (Geppert et al. 2006; Garrod & Herbst 2006) and it is expected to form efficiently starting from hydrogenation of CO (Hidaka et al. 2004) and to be abundant in those comets that formed in regions of the disk beyond the CO snowline. Recent studies (Qasim et al. 2018) suggest that

CH_3OH formation is possible also during earlier phases of interstellar ice evolution, through the sequential surface reaction chain: $CH_4 + OH \rightarrow CH_3 + H_2O$ and $CH_3 + OH \rightarrow CH_3OH$, at 10 - 20 K in H_2O-rich dense regions. Methanol is much less volatile than CO, and its abundances are not expected to change much over the lifetime of a comet.

Hydrocarbons could build up from successive H-atom additions to the products of photo-dissociated larger molecules (Bosman et al. 2018 and references therein). In particular, methane may form from successive hydrogenation of C, CH_2, CH_3 photo-products and it is expected to accumulate in the ice form in the outer disk, beyond its snow-line. Later in time, when the dust begins to agglomerate and energetic radiation penetrates more efficiently into the disk, C_2H_6 can be produced via recombination of photodissociation products of methane (e.g., CH, CH_2). In addition, ethane can also form from hydrogenation of C_2H_2 (Hiraoka et al. 2000). The lower median value measured for acetylene with respect to C_2H_6 in our sample may reflect this process. An alternative path for hydrocarbon formation could be through destruction of PAHs in the molecular layer and successive freezing onto grains (Tielens 2013); this may also explain in part the high positive correlations that we observe among hydrocarbons.

Following Schwarz & Bergin 2014, ammonia is expected to form from successive hydrogenation of NH and can be abundant already at 5 au: the compact distribution that we observe, agrees with a common value shared among the comet population. This is true except for 04Q2 and 07N3, that show strongly depleted values compared to the other comets: it is not clear at the moment the reason for this enhanced depletion in these two comets. HCN should form instead via gas-phase reactions in warmer regions and then be quickly adsorbed into the grains; in colder regions the nitrogen is more likely to participate in the formation of NH_3 than HCN, so that the latter is expected to show a more dispersed distribution in the comet population, and a lower median value. However, NH_3 is easily incorporated into ammonium salts through reactions with organic acids on grains, even at temperatures below 30K, thereby limiting the abundance of free NH_3 that can be retained as a primary volatile in comets (Mumma et al. 2019; Poch et al. 2020; Altwegg et al. 2020). The search for by-products of ammonium salts in comae of active comets is expected to provide new insights on nitrogen chemistry in the coming years.

Finally, H_2CO is among the species that show the lowest abundances in our study probably related to formaldehyde as an intermediate product in the formation of CH_3OH from hydrogenation of CO. The depletion of H_2CO may be also related to sequestration in the form of polymeric formaldehyde, as was inferred from mass spectral measurements in comet Halley and spectral mapping of other comets (Meier et al. 1993; Cottin & Fray 2008).

3.2 Relative abundances of the volatile species in comets

3.2.1 Pie charts

We compared 18 comets[3] using double-level pie charts (see Figures 6 and 7).

The inner level of each pie considers chemical functional groups in the following way: 1) CO and H_2CO (Carbonyl and Aldehyde groups) – in red; 2) CH_3OH (Alcohol group) – in yellow; 3) C_2H_6, CH_4, C_2H_2 (Hydrocarbon group) – in green; 4) HCN (Nitrile group) – in blue. In the outer level, we describe instead each molecular species separately. In this first analysis we haven't included the

[3] We excluded 17P and 10P since we don't have any measurements for CO and CH_4.

244 NH_3 contribution; we show that in Figure 8 instead[4]. The proportions reported in the pies are
245 obtained by normalizing each mixing ratio to the sum of all considered mixing ratios.

246 From the pie charts, we notice that even if the analyzed comets show a variety of different
247 compositions, they can be divided into two main groups. Comets 99S4, 09P1, 99T1, 13R1, 12F6,
248 04Q2 and 12S1 show a high amount of carbonyl material with respect to other functional groups.
249 Except for 99S4, the amount of methanol in these comets is comparable to that of the
250 hydrocarbon group. Methane is the dominant species among the hydrocarbons, with MRs that
251 are about twice that of C_2H_6 (except for comet 12S1). The second group of pies instead, show a
252 lower amount of CO and can be divided in two subgroups: while 07N3, and 99H1 still show a
253 higher amount of CH_4 with respect to ethane, the other comets show a comparable or higher
254 amount of the latter with respect to CH_4, with comet 01A2 showing an enrichment for this
255 species.

256 It could be possible that comets of the first group formed in a warmer region of the midplane,
257 where CH_3OH and hydrocarbons were not efficiently produced (Geppert et al. 2006; Garrod et
258 al. 2006), and CO and CH_4 were trapped in dust grains and sufficiently shielded from the radiation
259 field by the dust (Kama et al. 2016), so that these comets may have incorporated less chemically
260 processed material. On the other hand, comets belonging to the second group show proportions
261 of material that could be indicative of efficient hydrogenation processes, suggesting that these
262 comets formed in colder environments (Hiraoka et al. 2005). Comets that show a higher amount
263 of ethane with respect to methane, suggest the incorporation of material that could have been
264 significantly processed by the radiation field and later converted to ethane via successive
265 hydrogenations (see Bosman et al. 2018 and references therein).

266 When including the contribution of ammonia, we see basically the same grouping of comets:
267 13R1, 09P1, 12F6, 04Q2, 99S4 and 12S1 still show CO as the dominant molecular species, but
268 while 13R1, 09P1, 12S1 and 12F6 show a similar amount of NH_3, and the sum of nitriles
269 comparable with the sum of hydrocarbons, 04Q2 looks much depleted in ammonia. The value
270 shown in 99S4 is a 2σ upper limit, and we cannot exclude that it could be indeed the same as
271 the other comets in this group; for all these comets HCN always shows a lower value with respect
272 to ammonia. This could be the signature of formation of ammonium cyanide salt on grains in
273 regions where NH_3 formation exceeds that of HCN.

274 Comets in the second group display comparable to higher amounts of NH_3 with respect to C_2H_6
275 and CH_4, and in some cases some of the highest proportions for this molecule (see for example
276 comets 8P and 9P). Exceptions to this rule are comets 07N3 and 01A2, which instead show a very
277 low amount of ammonia. We also observe on average higher proportions of ammonia with
278 respect to HCN; on the other side, HCN proportions tends to be higher with respect to those in
279 the previous group, especially considering comets 73PB and 73PC.

280 **3.2.2 Correlations between relative abundance ratios and orbital parameters**

281 Considering the distribution of molecular species in comets inferred through the pie charts, we
282 wanted to investigate the interrelationships of multiple species, simultaneously. To do so, we
283 calculated and compared all the ratios of MRs relative to selected molecular species (CH_3OH, CO,
284 NH_3, C_2H_6 and CH_4), and retrieve their Spearman's correlation factors that we report in Table 5,
285 together with the corresponding statistics. Hereafter we describe three particular cases.

[4] We excluded comet 99T1 because the 2σ upper limit for NH_3 is not significant with respect to our statistic.

In Figure 9 we show the relationships between MR(CH_3OH)/MR(CO) (hereafter CH_3OH/CO) and MR(C_2H_6)/MR(CH_4) (hereafter C_2H_6/CH_4), along with corresponding graphs of these two ratios with respect to the Tisserand Invariant, the perihelion distance, and the inclination of the orbit. The colors scale with the values of the Tisserand invariant ($-2 < T_J < -0.6$ red; $-0.6 < T_J < 0.6$ yellow; $0.6 < T_J < 2$ green; $T_J > 2$ blue). It is possible to group tentatively our comet sample in the following way:

Group 1: 99H1 and 07N3: comets that have $-2 < T_J < -0.6$. They both show MRs of CH_3OH higher than those of CO, and the MRs of C_2H_6 lower than those of CH_4, being at the same time characterized by a high inclination.

Group 2: 09P1, 12F6, 99T1, 13R1: these comets are all characterized by low values for both CH_3OH/CO and C_2H_6/CH_4 ratios, and $-0.6 < T_J < 0.6$, with perihelion distances between about 0.6 and 1.6 au and medium to high inclinations.

Group 3: 01A2, 07W1 and 8P, that have $0.6 < T_J < 2$, perihelion distance from about 0.7 to 1 au, and inclinations lower than 50 deg. These comets show high values for both CH_3OH/CO and C_2H_6/CH_4 ratios.

Jupiter family comets ($2 < T_J < 3$) show a spread of the two different ratios, but many CH_4 and CO MRs correspond to 2σ upper limits, so that it is not possible to constrain in a proper way their nature considering only our dataset.

Exceptions to this grouping are comet 99S4 that has orbital parameters similar to those of 99H1 and 07N3 (group 1) but seems to belong to the second group; comet 00WM1 that acts as the third group even if its orbital parameters are similar to the second group; comet 04Q2, that shows many similarities with the second group even if dynamically it is more like the third group. It is not possible to infer from our data if these three comets represent a transition between different groups, or different groups by themselves.

If we substitute HCN for CH_3OH, we obtain very similar tendencies, as shown in Figure 10; in particular, comets in Group 2 show lower values of MR(HCN)/MR(CO) (hereafter, HCN/CO) with respect to comets in Group 3. In this case comet 99H1 is the one that differs from 07N3 and 99S4 (even so, we kept the color codes used in the previous figure). Also, it is possible to notice how the ratios HCN/CO and C_2H_6/CH_4 are well determined and lie in narrow intervals for Group 2, while they are more dispersed for the other groups.

Finally, in Figure 11, we tested MR(CH_3OH)/MR(NH_3) vs MR(HCN)/MR(C_2H_6) (hereafter CH_3OH/NH_3 and HCN/C_2H_6, respectively), that show a strong negative correlation, and a similar clustering of comets, with 09P1, 12F6 and 13R1 showing higher HCN/C_2H_6 abundance ratios and lower CH_3OH/NH_3 values with respect to other OC comets. In this case, it was also possible to include in the analysis JF comets: even if the ratios for these comets agree with the negative correlation trends of the OC comets, the relative MRs ratios with respect to their orbital parameters do not seem to follow any particular rule, and their values are quite spread, especially considering the HCN/C_2H_6 ratio.

The previous three examples agree and improve the classification produced using the pie charts and show that in principle it may be possible to relate the chemical composition of comets to their dynamical properties.

3.2.3 Testing the origins and chemical evolution of comets

Pondering the combination analyzed in Figure 9, i.e. MR(CH_3OH)/MR(CO) vs MR(C_2H_6)/MR(CH_4), we attempted to compare our results with some of the possible links expected for the same molecules within different disk regions, where comets may have formed (see Figure 12). We followed mainly the disk model described in Bosman et al, 2018: here, the authors explain the depletion of CO observed with ALMA in a large portion of proto-planetary disks as the result of the spatial and temporal evolution of CO, and they describe in detail the possible chemical connections among CO, CH_3OH, CH_4 and C_2H_6 (similar considerations can be found in Walsh et al. 2010; Eistrup et al. 2016, 2018). A general discussion should consider the positions of the molecular "snow lines" as a function of the luminosity of the central star (e.g. T-Tauri vs HAe disks (see for example Walsh et al. 2015; Wei et al. 2019) and of the evolutionary stages of the disks (see for example Garaud & Lin 2007; Oka et al. 2011; Piso et al. 2015; Ruaud & Gorti 2019). Here, as a simplification, we will assume that the CH_4 snowline locate at about 17 au, while the CO one at 25 au: these are considered "typical" midplane temperature profiles for a disk around a solar-mass star (see for example Bergin & Cleeves 2018 and references therein). We can identify four different scenarios:

1. **Comets that formed between 5 au and the methane snowline (assumed at about 17 au)**. This region should reflect a chemistry dominated by gas-phase processes, and correspond to the region where part of the Oort Cloud comets formed (Levison & Morbidelli 2003; Gomes et al. 2005). In this region CO is mainly gaseous, even if it can be trapped in the ice form in dust grains (Kama et al. 2016). An efficient gas-phase formation route for CO conversion to methanol is lacking (Geppert et al. 2006), so that the latter is expected to be scarce. At temperatures of a few hundred K, the C^+ channel can produce gas-phase CH_4 (Aikawa et al. 1999), which in the gas form is expected to be successively destroyed via photodissociation by cosmic-ray induced photons, in favor of CO_2 and/or unsaturated hydrocarbons, such as gas phase C_2H_4. Ethylene will in turn freeze onto grains and be hydrogenated to ethane, that may become particularly abundant (Dodson-Robinson et al. 2018). A comet formed in this region is expected to be characterized by mixing ratios of CH_3OH lower than those of CO and mixing ratios of C_2H_6 higher than those of methane, that would place it in the upper left quadrant of the graph in Figure 12 – panels B and C. None of the comets presented in this paper fall in this scenario.
2. **Comets that formed between the methane and CO snowlines (between about 17 au to 25 au).** Both Oort Cloud and Jupiter Family comets may have formed in this region of the disk. As in the case before, CO is still mainly in the gas state and CH_3OH is not forming efficiently. On the other hand, the temperatures drop below the CH_4 snowline, and methane will freeze and be abundant in grains. Comets formed in this region are expected to be characterized by mixing ratios of CO higher than the ones of CH_3OH and mixing ratios of CH_4 higher than the ones of C_2H_6, that cannot form efficiently through hydrogenation of photo-products of CH_4. That would place them in the lower left quadrant of the graphs. Comets like 99S4, 13R1, 09P1, 12F6, 04Q2 fall in this region, and they are all characterized by a ratio MR(CH_4):MR(C_2H_6) ~ 2:1, while comet 99T1 shows a higher ratio coupled with a very high amount of CO, suggesting a possible different origin for this comet, or highly efficient preservation mechanisms in the disk for the most volatile species.
3. **Comets that formed beyond the CO snowline (at distances longer than 25 au) early stages of the disk.** Comets that formed in this region (part of the OC comets) should be

characterized by material produced mainly through hydrogenation on grain surfaces. The final product of successive hydrogenations of CO is CH_3OH, that will be particularly enriched in the early stage of the disk lifetime (the first 3 Myr). Methanol is then expected to be photo-processed in favor of CH_4, that will become one of the most abundant hydrocarbons after 5 Myr. Comets that formed in this region before 5 Myr are expected then to show relative abundances of CO lower than methanol and $MR(CH_4) > MR(C_2H_6)$ and they should locate in the lower right quadrant of the graph in Figure 12 – panels B and C (in our case comets 07N3 and 99H1).

4. **Comets that formed beyond the CO snowline (at distances longer than 25 au) in a later stage of the disk.** After about 5 Myr, methane will decrease in favor of C_2H_6 (for a detailed explanation of these processes see Bosman et al. 2018 and references therein). Some of the comets that formed at distances > 25 au but collected processed material that formed later in time, are expected to show instead $MR(CH_4) < MR(C_2H_6)$ and should locate in the upper right quadrant (01A2, 00WM1, 07W1). In this group we may also find comets that formed earlier, but that could incorporate material coming from the molecular layer, where the chemistry of hydrocarbons is much enhanced (see for example Schwartz et al, 2018 and references therein).

The spread of locations of JF comets in the graph is probably a combination of both the original composition and the loss of the most volatile species during multiple revolutions around the Sun, as well as of the lack of precise measurements of CH_4 and CO for this dynamical family.

If we consider the bundle of straight lines $K = (MR(CH_3OH)*MR(C_2H_6))/(MR(CH_4)*MR(CO))$, see Figure 12 – panel B, we can associate an increasing K to the increasing formation distance of the comet from the proto-Sun (mainly for long period comets) and/or to a post-formation evolution of the cometary material (mainly but not only for short period comets). In fact, we expect a higher contribution of CH_3OH and C_2H_6 especially for those comets where hydrogenation processes were efficient (low temperatures). In this way we can assume for example that comets like 99S4, 13R1, 09P1, probably formed closer to the proto-Sun, while comets like 01A2, 00WM1 and 07W1 formed at larger distances, beyond the CO snowline.

In a similar way, if we trace the lines $M = (MR(CH_3OH)*MR(CH_4))/(MR(C_2H_6)*MR(CO))$, see Figure 12 – panel C, we can associate to each comet a second factor, whose value could be indicative of process of material by UV-X-CR radiation and successive H-atom addition during a later stage of the disk, with a lower value of M indicative of high efficiency in this process. Considering our sample, for example 00WM1, 07W1 and 01A2 share about the same K, but the lower value for M in 01A2 suggest that the material in this comet may have experienced higher photolysis. K and M factors are reported in Table 6.

4. Conclusions

We presented updated mixing ratios (% with respect to water) for 20 comets observed with NIRSPEC at the Keck Observatory since 1999. The results were obtained using modern and advanced fluorescence quantum band models and analysis techniques. We performed a descriptive statistic and correlation analysis on these results, trying to connect the abundances observed in these comets to the possible origin and evolution of the nucleus material in the proto-planetary disk.

Our analysis reveals that the composition of comets does not reflect a single dominant chemical process that could be present in the region where they formed, but rather a combination of chemical-physical processes (e.g. radical-radical reactions, hydrogenation, vertical mixing) which influence the different portions of the disk midplane during time; moreover, modification of the surface material of a nucleus after its formation may exist, especially for short period comets.
We identified two main chemical classes using pie charts, one compatible with less processed material and the other reflecting a different formation or possible evolution of the nucleus material with time.
We demonstrated that the quotients of different MRs can be more appropriate for developing a chemical classification, since they can reveal trends and similarity among comets not visible when comparing absolute values. In this way, we developed an alternative classification, still compatible with the pie-chart approach, and somehow correlated to the orbital parameters of the analyzed comets. However, exceptions are present, and our dataset is still small to confirm these trends in comets and to locate precisely short period comets in this scenario.
Finally, we compared our results with recent proto-planetary disk models, considering in particular the interrelationship between MR(CH_3OH)/MR(CO) and MR(C_2H_6)/MR(CH_4), and we defined two factors, K and M, that can be associated with an increasing processing of the cometary material in time and/or to an increasing formation distance of a comet (for long period comets), as well as to a post-evolution of the most volatile species (for short period comets). Depending on the K and M factors we can try to reconstruct the chemical and physical history of each analyzed comet.

These studies are based on a limited sample and they give a quite simplified view of the formation of comets, so that it is still not possible to unequivocally trace back the origins of the selected targets, neither to produce a firm taxonomical classification for these bodies. The addition of new objects to the presented sample is expected to change, at least in part, our statistics, and to help in understanding if biases are present (e.g. MRs influenced by the heliocentric distances). Nevertheless, the statistics presented here offer the possibility to investigate the origin and evolution of the cometary material in an alternative way.

Acknowledgments: *This work was supported by the NASA Astrobiology Institute (13-13NAI7-0032 to Goddard Space Flight Center, PI: M. J. Mumma) and the NASA Emerging Worlds Program (EW15-57 to Goddard Space Flight Center, PI: G. L. Villanueva). This research has made use of the Keck Observatory Archive (KOA), which is operated by the W. M. Keck Observatory and the NASA Exoplanet Science Institute (NExScI), under contract with the National Aeronautics and Space Administration. The authors wish to recognize and acknowledge the very significant cultural role and reverence that the summit of Maunakea has always had within the indigenous Hawaiian community. We are most fortunate to have the opportunity to conduct observations from this mountain.*

References

Aikawa, Y., Umebayashi, T., Nakano, T., & Miyama, S. M. 1999, ApJ, 519, 705, doi: 10.1086/307400

Altwegg, K., Balsiger, H., Hänni, N., et al. 2020, Nature Astronomy, 4, 533, doi: 10.1038/s41550-019-0991-9

Bergin, E. A., & Cleeves, L. I. 2018, Chemistry During the Gas-Rich Stage of Planet Formation, 137, doi: 10.1007/978-3-319-55333-7 137

Bockelée-Morvan, D., & Biver, N. 2017, Philosophical Transactions of the Royal Society of London Series A, 375, 20160252, doi: 10.1098/rsta.2016.0252

Bonev, B. P., Villanueva, G. L., DiSanti, M. A., et al. 2017, AJ, 153, 241, doi: 10.3847/1538-3881/aa64dd

Bosman, A. D., Walsh, C., & van Dishoeck, E. F. 2018, A&A, 618, A182, doi: 10.1051/0004-6361/201833497

Cottin, H., & Fray, N. 2008, SSRv, 138, 179, doi: 10.1007/s11214-008-9399-z

Dello Russo, N., Kawakita, H., Vervack, R. J., & Weaver, H. A. 2016, Icarus, 278, 301, doi: 10.1016/j.icarus.2016.05.039

Dodson-Robinson, S. E., Evans, Neal J., I., Ramos, A., Yu, M., & Willacy, K. 2018, ApJL, 868, L37, doi: 10.3847/2041-8213/aaf0fd

Eistrup, C., Walsh, C., & van Dishoeck, E. F. 2016, A&A, 595, A83, doi: 10.1051/0004-6361/201628509

Eistrup, C., Walsh, C., & van Dishoeck, E. F. 2018, A&A, 613, A14, doi: 10.1051/0004-6361/201731302

Faggi, S., Mumma, M. J., Villanueva, G. L., Paganini, L., & Lippi, M. 2019, AJ, 158, 254, doi: 10.3847/1538-3881/ab4f6e

Furuya, K., & Aikawa, Y. 2014, ApJ, 790, 97, doi: 10.1088/0004-637X/790/2/97

Garaud, P., & Lin, D. N. C. 2007, ApJ, 654, 606, doi: 10.1086/509041

Garrod, R. T., & Herbst, E. 2006, A&A, 457, 927, doi: 10.1051/0004-6361:20065560

Geppert, W. D., Hamberg, M., Thomas, R. D., et al. 2006, Faraday Discussions, 133, 177, doi: 10.1039/B516010C

Gicquel, A., Milam, S. N., Coulson, I. M., et al. 2015, ApJ, 807, 19, doi: 10.1088/0004-637X/807/1/19

Gomes, R., Levison, H. F., Tsiganis, K., & Morbidelli, A. 2005, Nature, 435, 466, doi: 10.1038/nature03676

Hidaka, H., Watanabe, N., Shiraki, T., Nagaoka, A., & Kouchi, A. 2004, ApJ, 614, 1124, doi: 10.1086/423889

Hiraoka, K., Takayama, T., Euchi, A., Handa, H., & Sato, T. 2000, ApJ, 532, 1029, doi: 10.1086/308612

Hiraoka, K., Wada, A., Kitagawa, H., et al. 2005, ApJ, 620, 542, doi: 10.1086/426958

Kama, M., Bruderer, S., van Dishoeck, E. F., et al. 2016, A&A, 592, A83, doi: 10.1051/0004-6361/201526991

Levison, H. F., Duncan, M. J., Brasser, R., & Kaufmann, D. E. 2010, Science, 329, 187, doi: 10.1126/science.1187535

Levison, H. F., & Morbidelli, A. 2003, Nature, 426, 419, doi: 10.1038/nature02120

Lippi, M., Villanueva, G. L., Mumma, M. J., et al. 2020, AJ, 159, 157, doi: 10.3847/1538-3881/ab7206

McLean, I. S., Becklin, E. E., Bendiksen, O., et al. 1998, in Society of Photo-Optical Instrumentation Engineers (SPIE) Conference Series, Vol. 3354, Infrared Astronomical Instrumentation, ed. A. M. Fowler, 566–578, doi: 10.1117/12.317283

Meier, R., Eberhardt, P., Krankowsky, D., & Hodges, R. R. 1993, A&A, 277, 677

Mumma, M., Charnley, S., Cordiner, M., et al. 2019, in EPSC-DPS Joint Meeting 2019, Vol. 2019, EPSC–DPS2019–1916

Mumma, M. J., & Charnley, S. B. 2011, ARA&A, 49, 471, doi: 10.1146/annurev-astro-081309-130811

Mumma, M. J., Weaver, H. A., Larson, H. P., Davis, D. S., & Williams, M. 1986, Science, 232, 1523, doi: 10.1126/science.232.4757.1523

Mumma, M. J., Bonev, B. P., Villanueva, G. L., et al. 2011, ApJL, 734, L7, doi: 10.1088/2041-8205/734/1/L7

Oka, A., Nakamoto, T., & Ida, S. 2011, ApJ, 738, 141, doi: 10.1088/0004-637X/738/2/141

Piso, A.-M. A., Öberg, K. I., Birnstiel, T., & Murray-Clay, R. A. 2015, ApJ, 815, 109, doi: 10.1088/0004-637X/815/2/109

Poch, O., Istiqomah, I., Quirico, E., et al. 2020, Science, 367, aaw7462, doi: 10.1126/science.aaw7462

Pontoppidan, K. M., Salyk, C., Banzatti, A., et al. 2019, ApJ, 874, 92, doi: 10.3847/1538-4357/ab05d8

Qasim, D., Chuang, K. J., Fedoseev, G., et al. 2018, A&A, 612, A83, doi: 10.1051/0004-6361/201732355

Ruaud, M., & Gorti, U. 2019, ApJ, 885, 146, doi: 10.3847/1538-4357/ab4996

Schwarz, K. R., & Bergin, E. A. 2014, ApJ, 797, 113, doi: 10.1088/0004-637X/797/2/113

Schwarz, K. R., Bergin, E. A., Cleeves, L. I., et al. 2018, ApJ, 856, 85, doi: 10.3847/1538-4357/aaae08

Tielens, A. G. G. M. 2013, Reviews of Modern Physics, 85, 1021, doi: 10.1103/RevModPhys.85.1021

Villanueva, G. L., Smith, M. D., Protopapa, S., Faggi, S., & Mandell, A. M. 2018, JQSRT, 217, 86, doi: 10.1016/j.jqsrt.2018.05.023

Walsh, C., Millar, T. J., & Nomura, H. 2010, ApJ, 722, 1607, doi: 10.1088/0004-637X/722/2/1607

Walsh, C., Nomura, H., & van Dishoeck, E. 2015, A&A, 582, A88, doi: 10.1051/0004-6361/201526751

Wei, C.-E., Nomura, H., Lee, J.-E., et al. 2019, ApJ, 870, 129, doi: 10.3847/1538-4357/aaf390

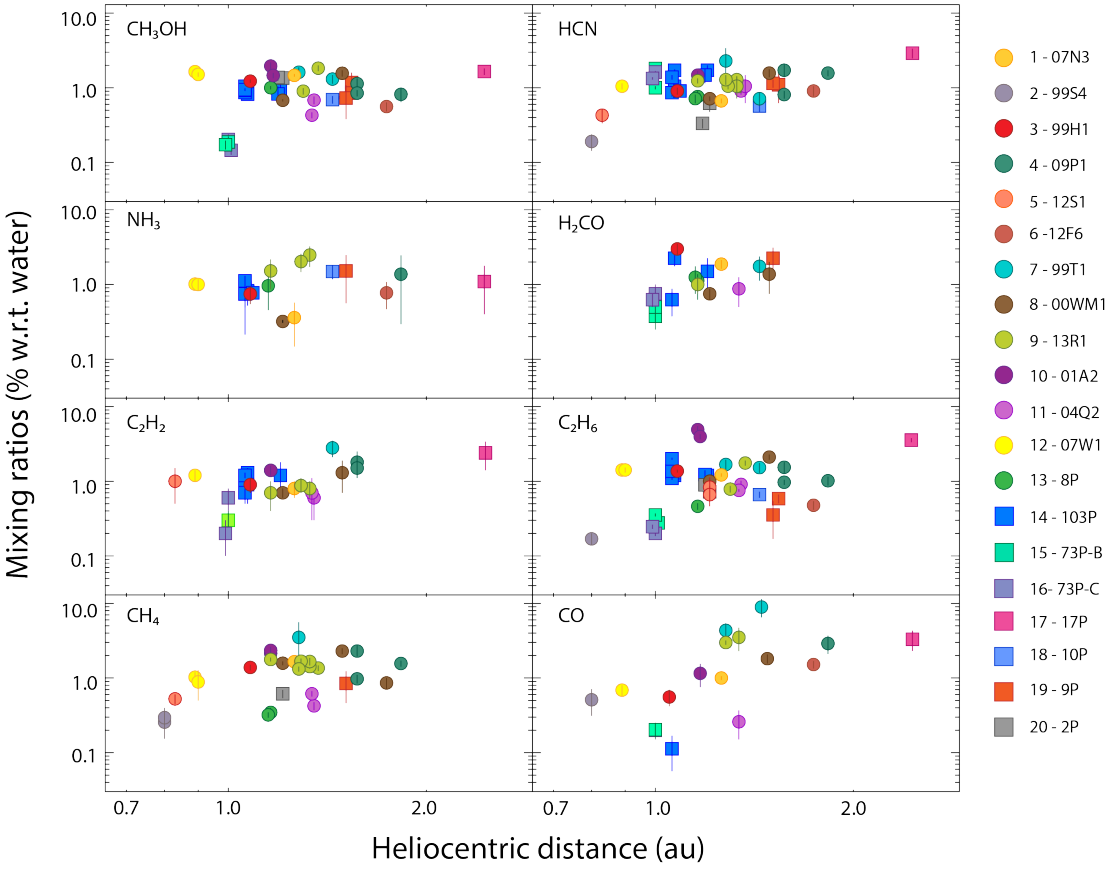

Figure 1: *Measured mixing ratios with respect to water (normalized to the median) with respect to the heliocentric distance at the time of observations for the studied comets. Each color represents a different comet as indicated in the color legend on the top of the graphic: The data are numbered according to increasing Tisserand Invariant (see Table 1). Upper limits are not reported.*

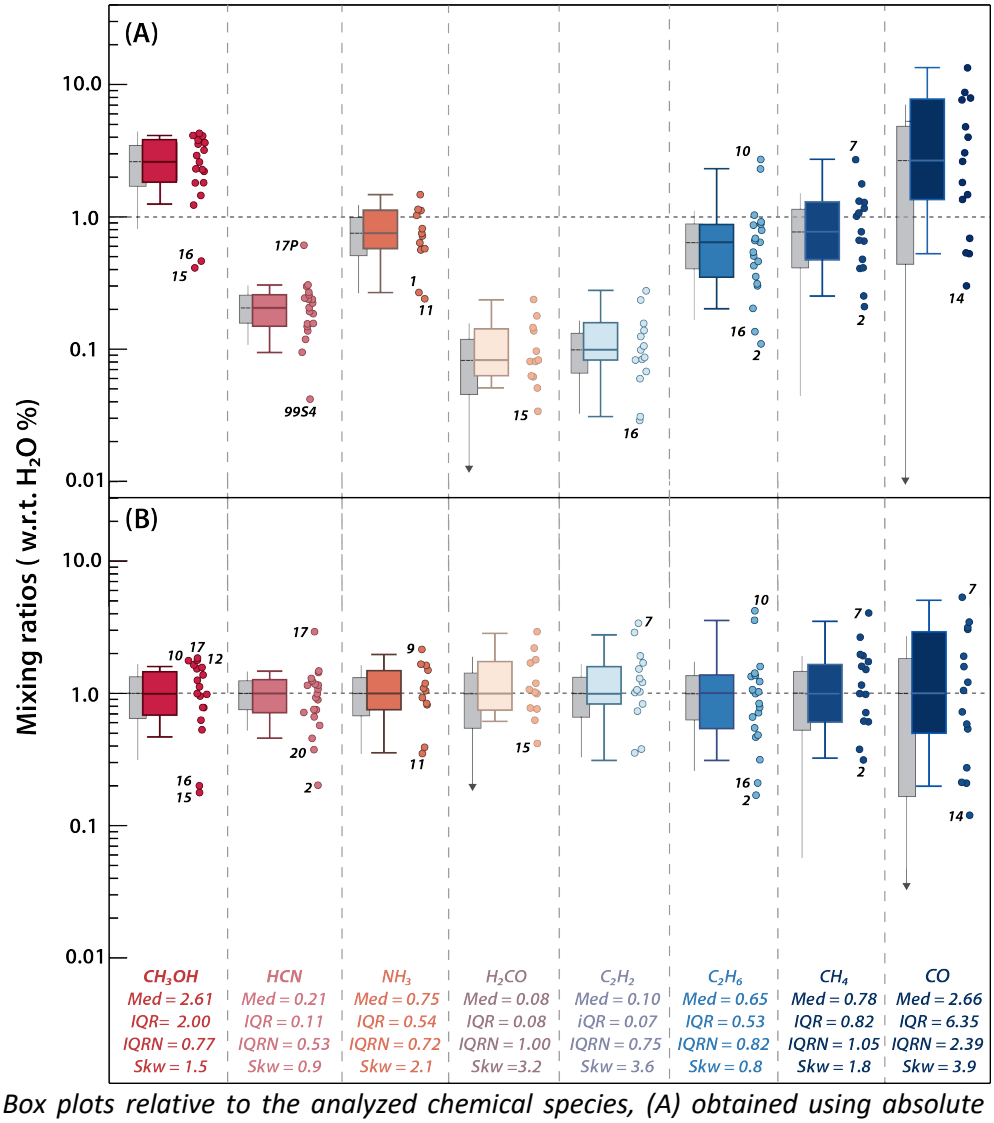

***Figure 2**: Box plots relative to the analyzed chemical species, (A) obtained using absolute values, (B) obtained using mixing ratios normalized to the median; the boxes are ordered and colored by sublimation temperature (red = higher temperatures, blue = lower temperatures). For each molecule, we report the median (Med), the Interquartile Range (IQR), the interquartile range normalized to the median (IQRN), and the skewness (Skw) of the distribution. The median is also indicated with a horizontal line across each box. The whiskers are calculated as the 9th and 91st percentiles. Comets that present outlier values with respect to the whiskers are highlighted with their individual number, following Table 1. Each box is compared with a gaussian distribution, represented as a grey box centered on the median and characterized by a standard deviation comparable to the interquartile range. The complete statistic for each box is reported in Table 3.*

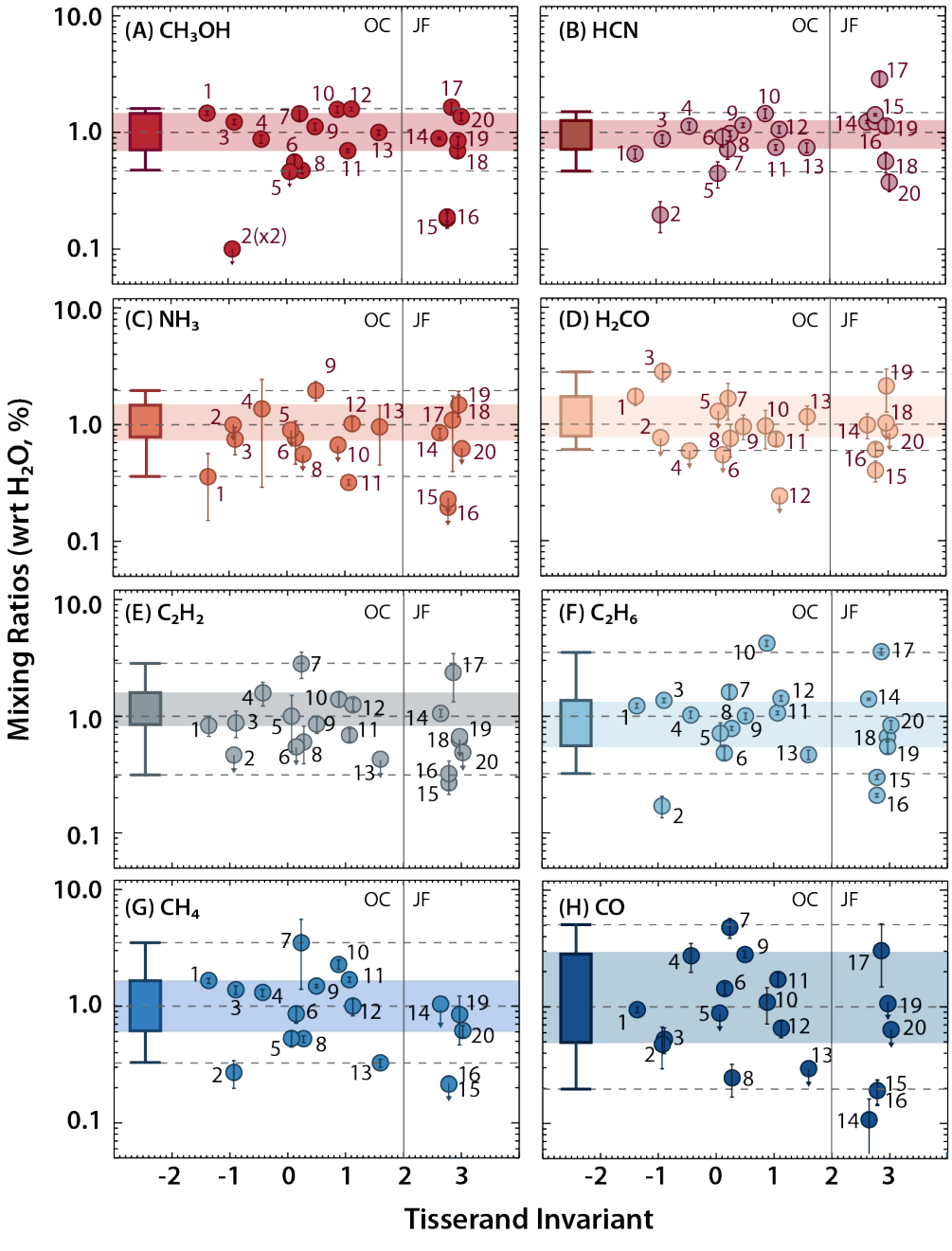

Figure 3: *Measured mixing ratios (normalized to the median values) as a function of the Tisserand invariant for the twenty comets. For each plot, the data are reported with their corresponding error bars; downward arrows represent 2σ upper limits (2σ upper limits that are not significant are not shown). The 25th and 75th percentiles are indicated as a colored horizontal bar, while medians, 9th and 91st percentiles are shown through horizontal dashed lines. A vertical solid line separates OC and JF comets. The data are numbered according to increasing Tisserand Invariant (see Table 1).*

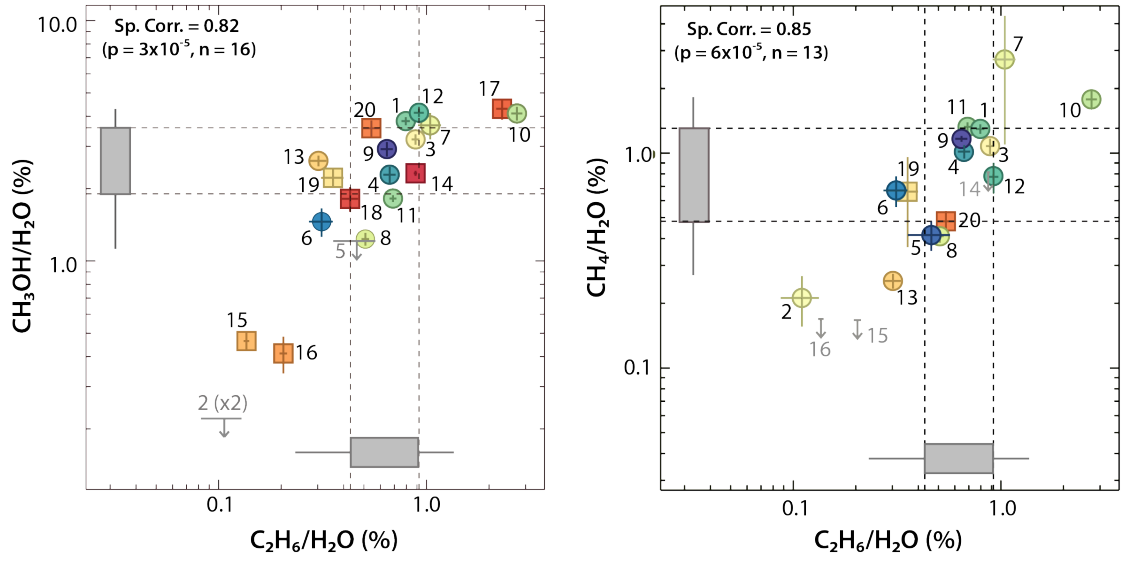

***Figure 4**: Examples of Spearman's correlation factors higher than 0.50 among different molecular species observed in our sample of comets. For each graph, circles indicate OC comets, while squares indicate JF comets; 2σ upper limits are shown with a gray arrow; the boxplots of the molecules are shown in grey for each axis and the Spearman's correlation coefficient and its statistic is reported in the upper left corner. The data are numbered following the increasing Tisserand Invariant (see Table 1).*

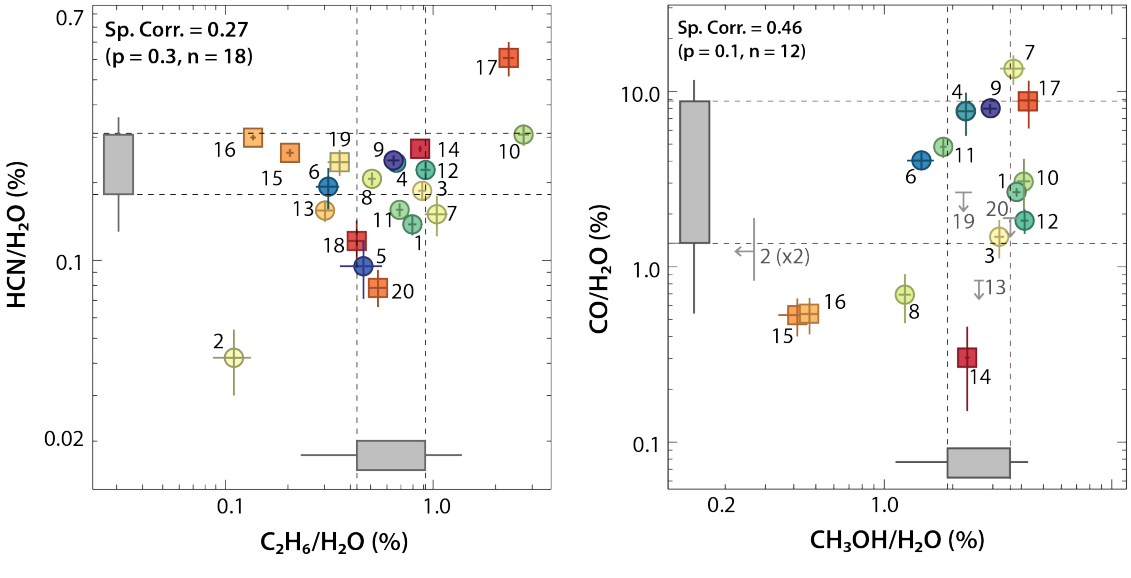

***Figure 5:** Examples of Spearman's correlation factors lower than 0.50 among different molecular species observed in our sample of comets. For each graph, circles indicate OC comets, while squares indicate JF comets; 2σ upper limits are shown with a gray arrow; the boxplots of the molecules are shown in grey for each axis and the Spearman's correlation coefficient and its statistic is reported in the upper left corner. The data are numbered following the increasing Tisserand Invariant (see Table 1).*

563

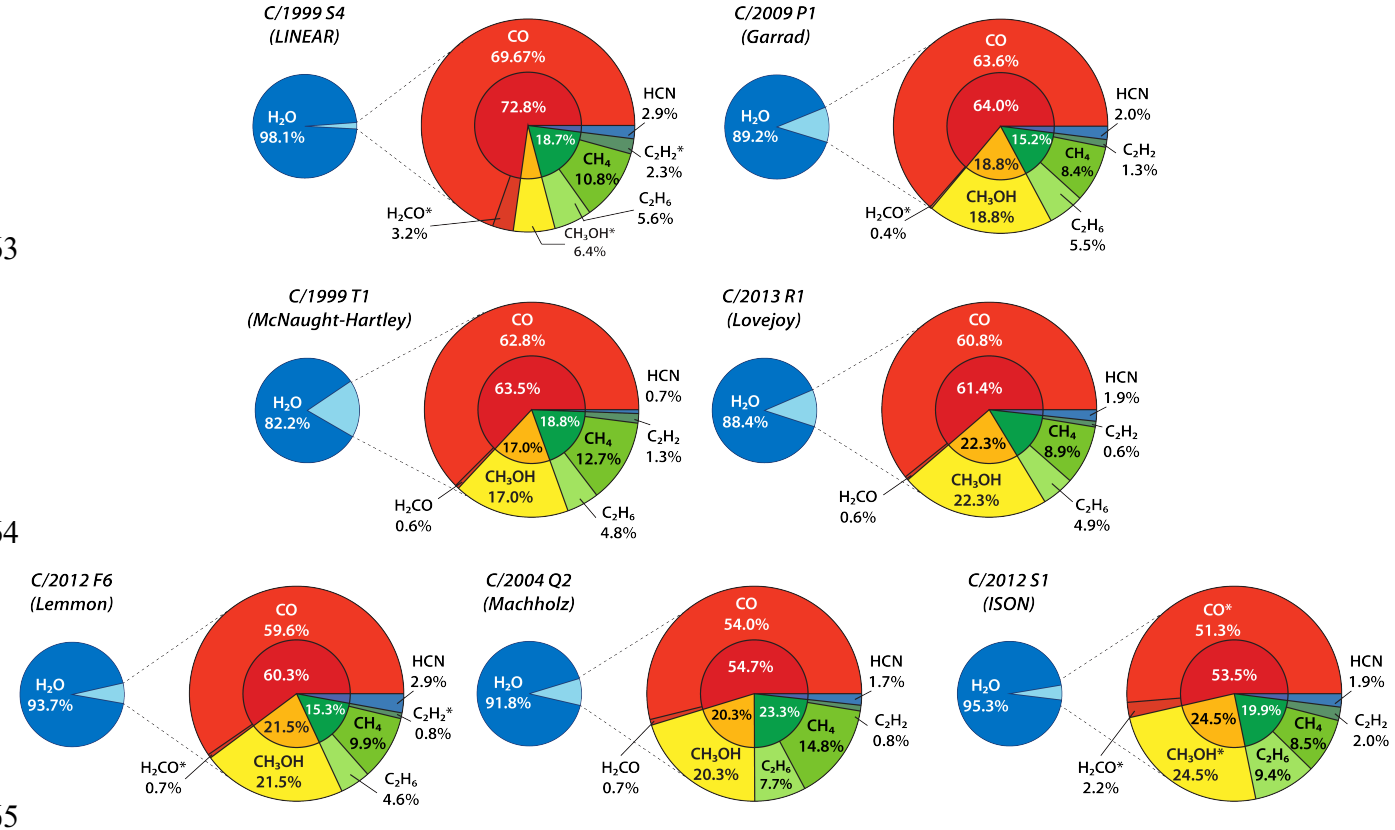

564

565

566 ***Figure 6***: *Two level pie charts for the analyzed comets, ordered with decreasing CO – First group. Different*
567 *colors indicate different functional group as follow: 1) CO and H_2CO (Carbonyl and Aldehyde groups) – in*
568 *red; 2) CH_3OH (Alcohol group) – in yellow; 3) C_2H_6, CH_4, C_2H_2 (Hydrocarbons group) – in green; 4) HCN*
569 *(Nitrile group) – in blue. For each molecule the reported proportion is obtained normalizing the*
570 *corresponding mixing ratio to the sum of all the considered mixing ratios obtained for that particular*
571 *comet. Starred labels represent 2σ upper limits.*

572

573

574

575

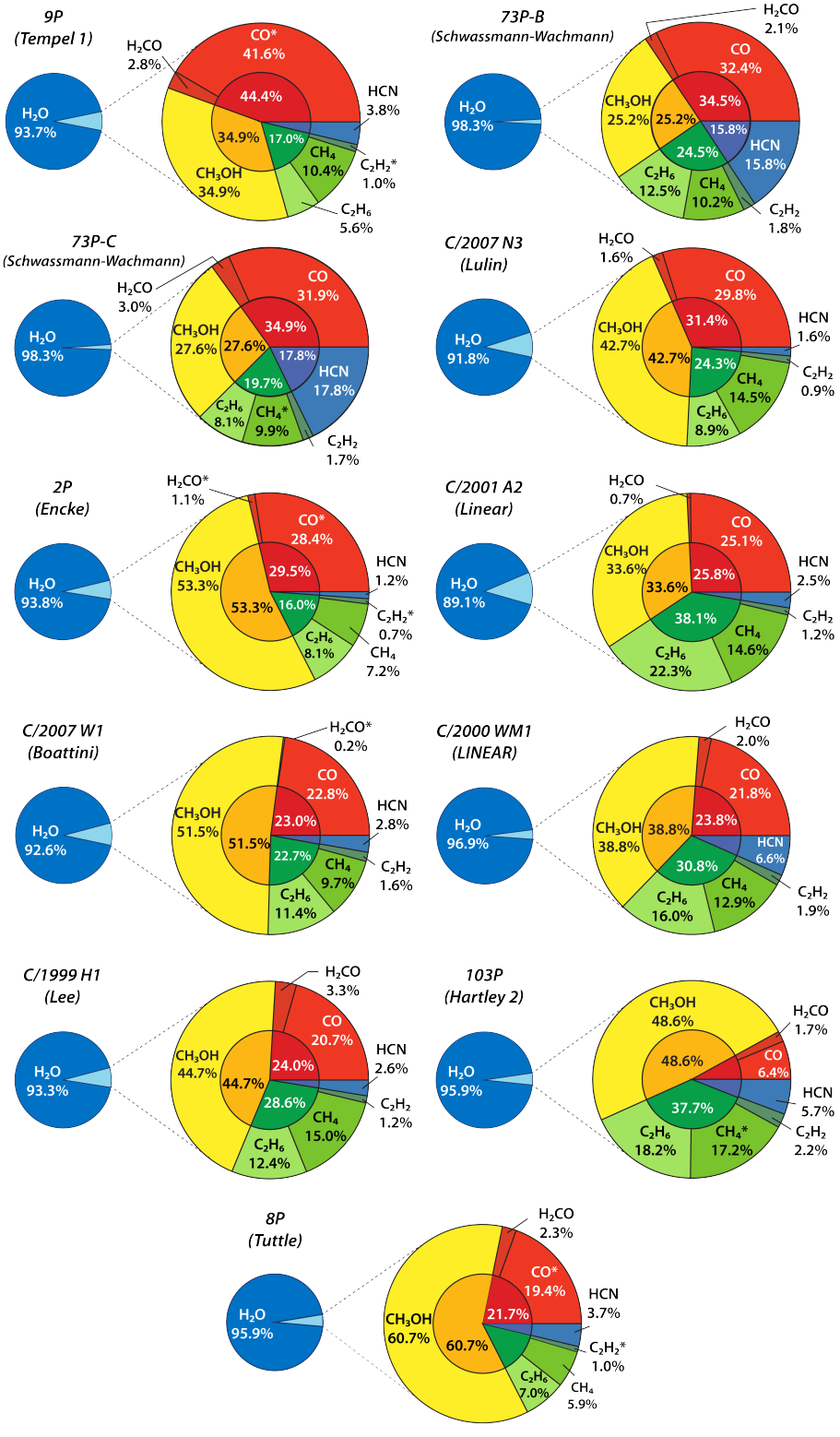

***Figure 7**: Two level pie charts for the analyzed comets, ordered with decreasing CO – Second group. Different colors indicate different functional group as follow: 1) CO and H_2CO (Carbonyl and Aldehyde groups) – in red; 2) CH_3OH (Alcohol group) – in yellow; 3) C_2H_6, CH_4, C_2H_2 (Hydrocarbons group) – in green; 4) HCN (Nitrile group) – in blue. For each molecule the reported proportion is obtained normalizing the corresponding mixing ratio to the sum of all the considered mixing ratios obtained for that particular comet. Starred labels represent 2σ upper limits.*

588
589
590
591
592
593

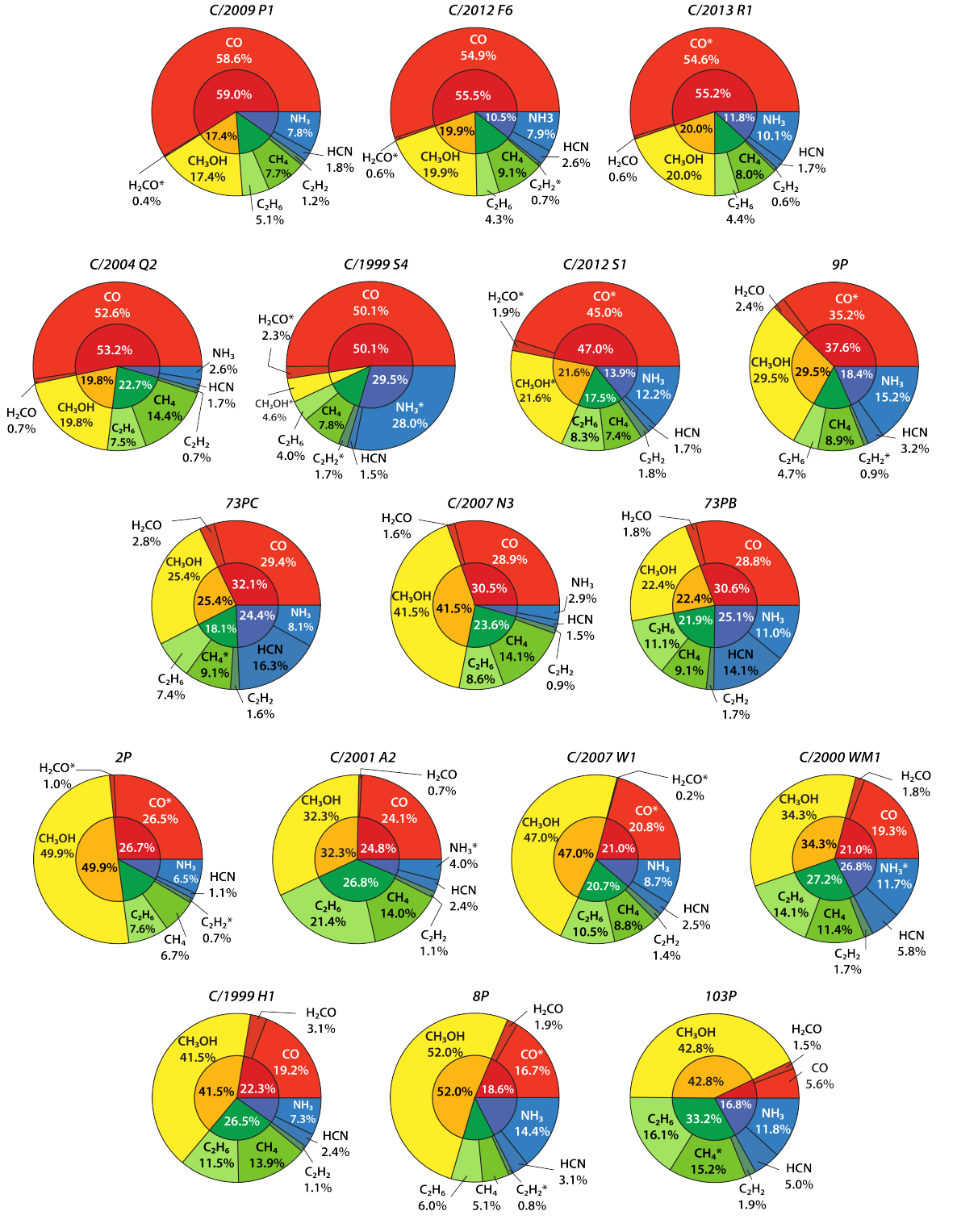

***Figure 8**: Two level pie charts for the analyzed comets, ordered with decreasing CO – including NH_3. Different colors indicate different functional group as follow: 1) CO and H_2CO (Carbonyl and Aldehyde groups) – in red; 2) CH_3OH (Alcohol group) – in yellow; 3) C_2H_6, CH_4, C_2H_2 (Hydrocarbons group) – in green; 4) HCN (Nitrile group) – in blue. For each molecule the reported proportion is obtained normalizing the corresponding mixing ratio to the sum of all the considered mixing ratios obtained for that particular comet. Starred labels represent 2σ upper limits.*

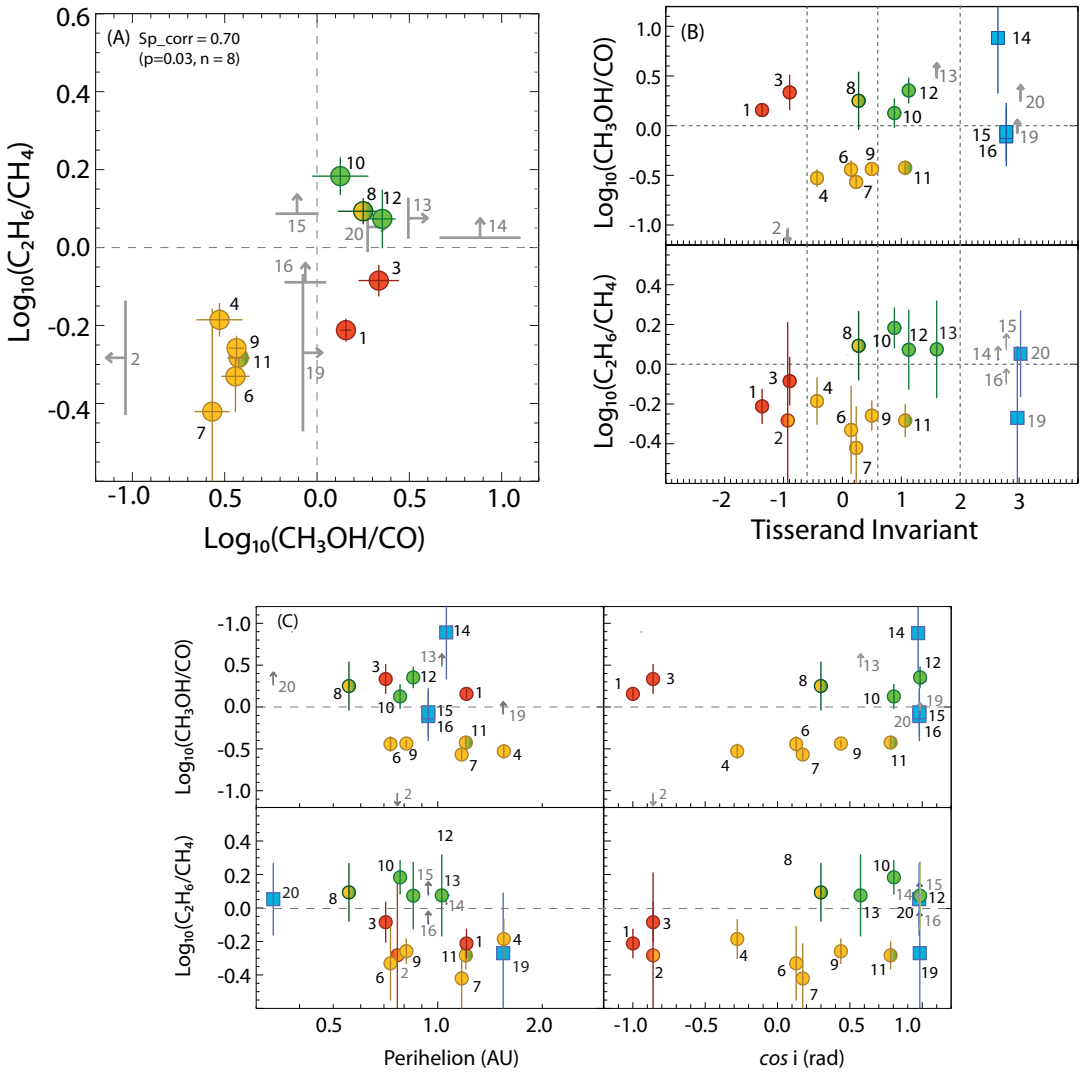

***Figure 9**: Comparison between: (A) MR(CH_3OH)/MR(CO) and MR(C_2H_6)/MR(CH_4) ratios (indicated in the plot as CH_3OH/CO and C_2H_6/CH_4, respectively); (B) same ratios versus the Tisserand Invariant; (C) same ratios vs the Perihelion and the inclination (i, radiants) of the orbit of the selected comets. In each panel, 2σ upper limits are shown with grey arrows and tags. In panel (A) we report the Spearman's correlation factor and its statistic, while colors are given considering possible clusters related to different chemical compositions; the same color scheme is used also in the other panels. Data are numbered following the increasing Tisserand Invariant.*

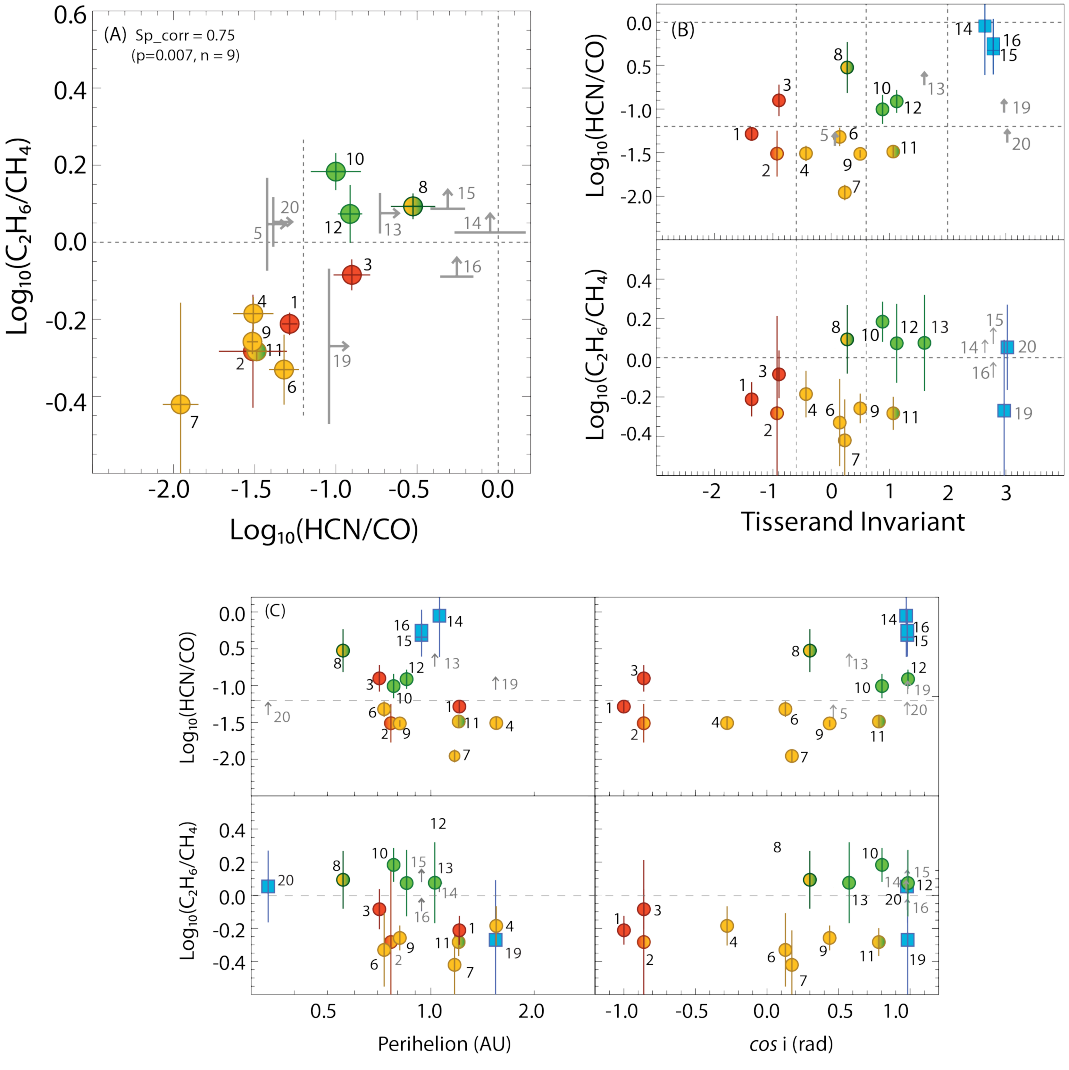

_Figure 10__: Comparison between: (A) MR(HCN)/MR(CO) and MR(C_2H_6)/MR(CH_4) ratios (indicated in the plot as HCN/CO and C_2H_6/CH_4, respectively); (B) same ratios versus the Tisserand Invariant; (C) same ratios vs the Perihelion and the inclination (i, radiants) of the orbit of the selected comets. In each panel, 2σ upper limits are shown with grey arrows and tags. In panel (A) we report the Spearman's correlation factor and its statistic, while colors are given considering possible clusters related to different chemical compositions; the same color scheme is used also in the other panels. Data are numbered following the increasing Tisserand Invariant._

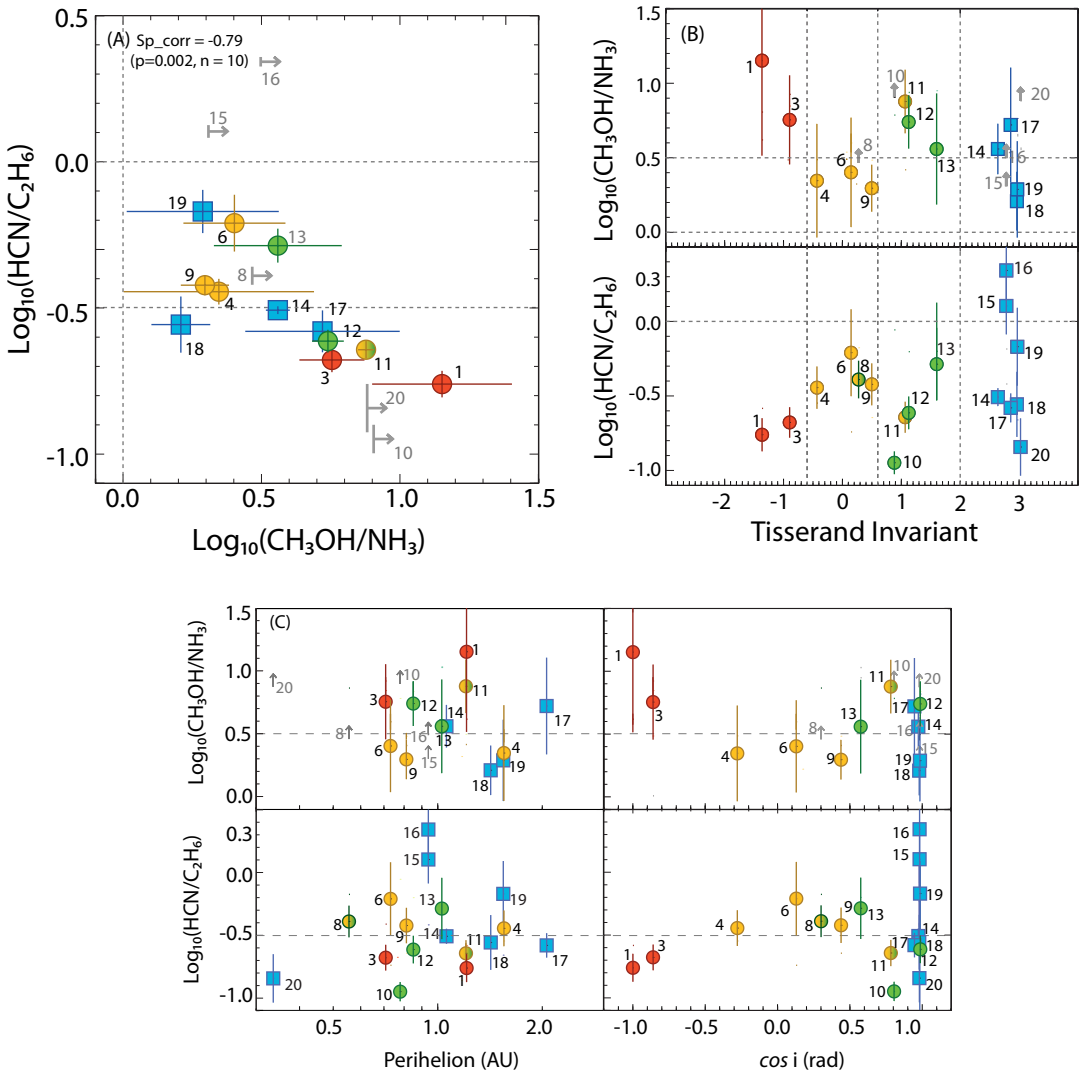

***Figure 11**: Comparison between: (A) MR(CH_3OH)/MR(NH_3) and MR(HCN)/MR(C_2H_6) ratios (indicated in the plot CH_3OH/NH_3 and HCN/C_2H_6, respectively); (B) same ratios versus the Tisserand Invariant; (C) same ratios vs the Perihelion and the inclination (i, radiants) of the orbit of the selected comets. In each panel, 2σ upper limits are shown with grey arrows and tags. In panel (A) we report the Spearman's correlation factor and its statistic, while colors are given considering possible clusters related to different chemical compositions; the same color scheme is used also in the other panels. Data are numbered following the increasing Tisserand Invariant.*

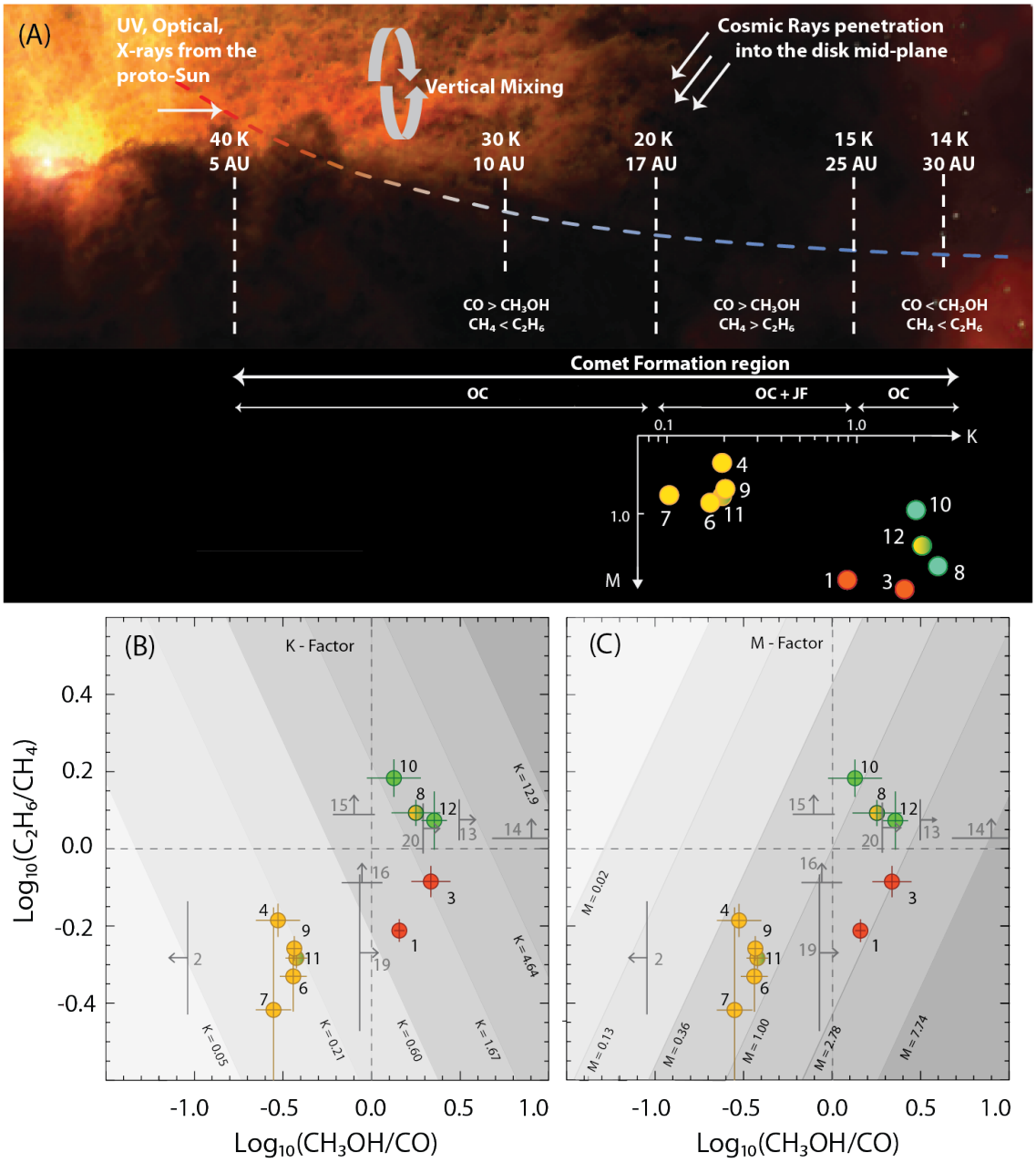

Figure 12: *Connections between protoplanetary disks and comets: in the upper panel we illustrate a scheme of the disk showing some of the major chemical-physical processes that involve the material that will be incorporated in cometary nuclei. In the lower panels, we show the relationship between* $MR(CH_3OH)/MR(CO)$ *and* $MR(C_2H_6)/MR(CH_4)$ *ratios (indicated in the plot as* CH_3OH/CO *and* C_2H_6/CH_4*, respectively) for the analyzed comets. In panels (B) and (C) a selection of the bundle of straight lines* $K = (MR(CH_3OH)*MR(C_2H_6))/(MR(CH_4)*MR(CO))$*, and* $M = (MR(CH_3OH)*MR(CH_4))/(MR(C_2H_6)*MR(CO))$ *are shown with grey scales.*

650 **Table 1: Observing logs and orbital parameters for the analyzed comets**

			Log for the observations				Orbital parameters		
	Comet[a]	Date range	R_h (au)	Δ (km s^{-1})	V_Δ (km s^{-1})	Dynamical Type[b]	T_j	q (au)	i (deg)
1	**07N3**	31 Jan 2009	1.26	0.95	-54.2	OC - DN	-1.37	1.21	178.4
		1 Feb 2009	1.26	0.92	-54.1				
2	**99S4**	13 Jul 2000	0.81	0.55	-54.6	OC – DN	-0.93	0.77	149.4
3	**99H1**	19 Aug 1999	1.05	1.38	-28.3	OC	-0.90	0.71	149.4
		20 Aug 1999	1.06	1.36	-29.0				
4	**09P1**	13 Oct 2011	1.83	1.84	19.2	OC – DN	-0.43	1.55	106.2
		9 Jan 2012	1.57	1.84	-20.9				
		10 Jan 2012	1.57	1.83	-21.2				
5	**12S1**	22 Oct 2013	1.21	1.50	-52.1	OC - DN	0.07	0.01	62.4
		24 Oct 2013	1.17	1.44	-51.6				
		25 Oct 2013	1.15	1.41	-51.4				
		7 Nov 2013	0.83	1.06	-42.0				
6	**12F6**	20 Jun 2013	1.74	1.79	5.4	OC	0.15	0.73	82.6
7	**99T1**	14 Jan 2001	1.28	1.35	-11.2	OC	0.23	1.17	80.0
		5 Feb 2001	1.44	1.29	1.6				
		6 Feb 2001	1.45	1.29	2.3				
8	**00WM1**	23 Nov 2001	1.35	0.38	-23.4	OC	0.28	0.56	72.6
		24 Nov 2001	1.34	0.37	-21.3				
9	**13R1**	22 Oct 2013	1.37	0.84	-40.0	OC	0.50	0.81	64.0
		24 Oct 2013	1.34	0.79	-39.5				
		25 Oct 2013	1.33	0.77	-39.0				
		27 Oct 2013	1.30	0.73	-38.2				
		28 Oct 2013	1.29	0.70	-37.7				
		29 Oct 2013	1.28	0.68	-37.2				
10	**01A2**	9 Jul 2001	1.16	0.28	11.4	OC	0.88	0.78	36.5
		10 Jul 2001	1.17	0.28	12.5				
11	**04Q2**	28 Nov 2004	1.49	0.66	-21.8	OC	1.07	1.21	38.6
		29 Nov 2004	1.48	0.64	-21.7				
		19 Jan 2005	1.21	0.39	11.2				
12	**07W1**	9 Jul 2008	0.89	0.35	12.9	OC – DN	1.13	0.85	9.9
		10 Jul 2008	0.90	0.36	13.0				
13	**8P**	22 Dec 2007	1.16	0.32	-19.2	HT	1.60	1.03	55.0
		23 Dec 2007	1.15	0.31	-18.0				
14	**103P**	16 Sep 2010	1.20	0.28	-12.0	JF	2.64	1.06	13.6
		18 Sep 2010	1.19	0.26	-11.7				
		17 Oct 2010	1.07	0.13	-2.3				
		19 Oct 2010	1.07	0.12	-0.9				
		21 Oct 2010	1.06	0.12	0.6				
		22 Oct 2010	1.06	0.12	1.2				
		4 Nov 2010	1.06	0.16	7.0				
		16 Nov 2010	1.09	0.21	8.7				
15	**73PB**	14 May 2006	1.00	0.07	0.3	JF	2.78	0.94	11.4
		15 May 2006	1.00	0.07	2.0				
16	**73PC**	14 May 2006	1.00	0.08	3.1	JF	2.78	0.94	11.4
		15 May 2006	1.00	0.08	4.6				
17	**17P**	27 Oct 2007	2.45	1.63	-3.3	JF	2.86	2.06	19.1
		30 Oct 2007	2.46	1.62	-2.3				
18	**10P**	26 Jul 2010	1.44	0.69	-4.2	JF	2.96	1.42	12.0
19	**9P**	3 Jun 2005	1.54	0.76	5.5	JF	2.97	1.54	10.5
		4 Jul 2005	1.51	0.89	9.2				
		5 Jul 2005	1.51	0.89	9.3				
20	**2P**	4 Nov 2003	1.21	0.31	-13.4	JF - ET	3.03	0.34	11.8
		5 Nov 2003	1.19	0.31	-12.5				
		6 Nov 2003	1.18	0.30	-11.5				

a) Comets are ordered with increasing Tisserand parameter; acronyms are described in footnote 1. b) JF = Jupiter Family, ET = Encke Type, HT = Halley Type, OC = Oort Cloud, DN = Dynamically new.

Table 2: Updated mixing ratios (% relative to water) measured for the selected comets

		Mixing ratios with respect to water %							
	Comet[a]	CH_3OH	HCN	NH_3	H_2CO	C_2H_2	C_2H_6	CH_4	CO
1	07N3	3.82 ± 0.15	0.14 ± 0.01	0.27 ± 0.16	0.15 ± 0.02	0.08 ± 0.02	0.80 ± 0.04	1.30 ± 0.07	2.66 ± 0.15
2	99S4	<0.13	0.04 ± 0.02	< 0.76††	< 0.06	< 0.05	0.11 ± 0.02	0.22 ± 0.06	1.36 ± 0.32
3	99H1	3.20 ± 0.16	0.19 ± 0.02	0.56 ± 0.15	0.24 ± 0.04	0.09 ± 0.02	0.89 ± 0.04	1.07 ± 0.09	1.48 ± 0.37
4	09P1	2.29 ± 0.18	0.24 ± 0.02	1.03 ± 0.81	< 0.05	0.16 ± 0.04	0.67 ± 0.05	1.02 ± 0.07	7.71 ± 2.13
5	12S1	< 1.2	0.10 ± 0.02	< 0.68	< 0.09†	0.11 ± 0.05	0.41 ± 0.09	0.41 ± 0.06	< 2.52
6	12F6 [b]	1.46 ± 0.20	0.19 ± 0.04	0.58 ± 0.23	< 0.05	< 0.05	0.31 ± 0.04	0.67 ± 0.11	4.03 ± 0.45
7	99T1	3.65 ± 0.38	0.15 ± 0.03	< 1.1†	0.14 ± 0.05	0.28 ± 0.07	1.04 ± 0.13	2.72 ± 1.63	13.48 ± 2.59
8	00WM1	1.23 ± 0.08	0.21 ± 0.01	< 0.42	0.06 ± 0.02	0.06 ± 0.02	0.51 ± 0.02	0.41 ± 0 .03	0.69 ± 0.22
9	13R1	2.92 ± 0.20	0.24 ± 0.01	1.48 ± 0.28	0.08 ± 0.01	0.08 ± 0.01	0.65 ± 0.04	1.17 ± 0.04	7.97 ± 0.51
10	01A2	4.11 ± 0.25	0.30 ± 0.02	< 0.51	0.08 ± 0.02	0.14 ± 0.02	2.73 ± 0.15	1.79 ± 0.17	3.07 ± 0.96
11	04Q2	1.82 ± 0.06	0.157 ± 0.009	0.24 ± 0.01	0.062 ± 0.008	0.068 ± 0.009	0.69 ± 0.03	1.32 ± 0.06	4.83 ± 0.66
12	07W1	4.13 ± 0.29	0.22 ± 0.02	0.76 ± 0.14	< 0.02	0.13 ± 0.02	0.92 ± 0.06	0.78 ± 0.15	1.83 ± 0.31
13	8P	2.61 ± 0.13	0.16 ± 0.02	0.72 ± 0.38	0.10 ± 0.02	< 0.04	0.30 ± 0.03	0.25 ± 0.02	< 0.84
14	103P [c]	2.32 ± 0.05	0.259 ± 0.007	0.64 ± 0.06	0.08 ± 0.02	0.105 ± 0.008	0.87 ± 0.01	< 0.8††	0.30 ± 0.15
15	73PB [d]	0.41 ± 0.05	0.259 ± 0.008	< 0.20	0.03 ± 0.01	0.03 ± 0.01	0.204 ± 0.008	< 0.17	0.53 ± 0.13
16	73PC [d]	0.47 ± 0.05	0.299 ± 0.007	< 0.15	0.051 ± 0.006	0.029 ± 0.009	0.136 ± 0.004	< 0.17	0.53 ± 0.13
17	17P [e]	4.30 ± 0.43	0.61 ± 0.09	0.82 ± 0.52	< 0.16†	0.24 ± 0.11	2.31 ± 0.14	N.A.	8.8 ±2.7
18	10P [f]	1.81 ± 0.21	0.12 ± 0.02	1.12 ± 0.24	< 0.09††	< 0.06	0.43 ± 0.04	N.A.	N.A.
19	9P	2.22 ± 0.19	0.24 ± 0.03	1.14 ± 0.72	0.18 ± 0.07	< 0.07	0.36 ± 0.04	0.66 ± 0.30	< 2.65
20	2P	3.56 ± 0.27	0.08 ± 0.01	< 0.47	< 0.07	< 0.05	0.54 ± 0.05	0.48 ± 0.06	< 1.9
	MEDIAN	**2.61**	**0.21**	**0.75**	**0.08**	**0.10**	**0.65**	**0.78**	**2.66**

a) Comets are ordered following increasing Tisserand parameter (see Fig. 1); b) CH_4 is from Paganini et al., 2014; c) CO in 103P is from Weaver et al., 2011; d) CO is taken from DiSanti et al., 2007 while CH_4 is from Villanueva et al., 2006; we used common values for both the fragments; e) it was not possible to measure CH_4 in 17P; f) it was not possible to measure CO and CH_4 in 10P; †) upper limit is much greater than the median, we consider it not significant; ††) upper limit is comparable to the median, we consider it significant.

Table 3: Boxplot statistics of the updated mixing ratios.

	CH_3OH	HCN	NH_3	H_2CO	C_2H_2	C_2H_6	CH_4	CO
Number of used points	18	20	12	12	14	20	15	15
9th percentile (normalized value)	1.23 (0.47)	0.10 (0.46)	0.27 (0.36)	0.05 (0.61)	0.03 (0.31)	0.20 (0.32)	0.25 (0.33)	0.53 (0.20)
25th percentile (normalized value)	1.82 (0.70)	0.15 (0.72)	0.58 (0.77)	0.07 (0.80)	0.08 (0.84)	0.36 (0.55)	0.48 (0.62)	1.36 (0.51)
Median - 50th percentile	2.61	0.21	0.75	0.08	0.10	0.65	0.78	2.66
75th percentile (normalized value)	3.82 (1.46)	0.26 (1.26)	1.12 (1.49)	0.15 (1.76)	0.16 (1.59)	0.89 (1.38)	1.30 (1.67)	7.71 (2.90)
91st percentile (normalized value)	4.14 (1.59)	0.31 (1.49)	1.48 (1.96)	0.24 (2.87)	0.28 (2.80)	2.31 (3.58)	2.72 (3.51)	13.48 (5.07)
Interquartile Range (IQR)	2.00	0.11	0.58	0.08	0.07	0.53	0.81	6.35
Normalized IQRN[a]	0.77	0.53	0.72	0.96	0.75	0.82	1.05	2.39
Skewness[b]	1.53	0.93	2.10	3.71	3.63	0.83	1.75	3.89
Average	2.57	0.21	0.78	0.10	0.11	0.75	0.95	3.95
Standard deviation	1.23	0.12	0.36	0.06	0.07	0.67	0.67	3.89
Min value	0.41	0.04	0.24	0.03	0.03	0.11	0.21	0.30
Max value	4.30	0.61	1.48	0.24	0.28	2.73	2.73	13.5

a) Normalized with respect to the median; b) calculated as (75th percentile – 50th percentile)/(50th percentile- 25th percentile).

Table 4: Spearman's correlations among the updated mixing ratios[a].

	CH_3OH	HCN	NH_3	H_2CO	C_2H_2	C_2H_6	CH_4	CO
CH_3OH	-	-0.02 0.9 16	-0.02 0.95 10	0.65 0.02 10	0.74 $4x10^{-3}$ 11	**0.82** **$3x10^{-5}$** **16**	0.45 0.1 11	**0.46** **0.09** **12**
HCN	-	-	0.41 0.18 10	-0.50 0.1 10	0.08 0.8 12	**0.26** **0.3** **18**	0.36 0.2 13	-0.10 0.7 13
NH_3	-	-	-	n.a[b]	n.a[b]	-0.25 0.4 10	-0.45 0.2 7	0.48 0.2 7
H_2CO	-	-	-	-	0.72 0.02 8	0.47 0.1 10	-0.13 0.7 7	0.30 0.4 8
C_2H_2	-	-	-	-	-	0.77 $1x10^{-3}$ 12	0.31 0.4 8	0.7 0.02 11
C_2H_6	-	-	-	-	-	-	**0.85** **$6x10^{-5}$** **13**	0.45 0.1 13
CH_4	-	-	-	-	-	-	-	0.65 0.03 9
CO	-	-	-	-	-	-	-	-

a) The first value in each cell represent the Spearman's correlation coefficient calculated excluding the upper limits; below the correlation coefficient, we report the (two-sided) level of significance (p) and the degrees of freedom of the calculation (n); cells with good statistic ($p \leq 0.05$ and $n \geq 9$) are highlighted in green; correlations in bold numbers are shown in figures 4 and 5 and discussed in the text; b) the degrees of freedom are less than 5 and considered too few for a good statistic.

Table 5: Spearman's correlations among ratios of the updated mixing ratios[a].

	$\frac{CH_3OH}{HCN}$	$\frac{CH_3OH}{NH_3}$	$\frac{CH_3OH}{C_2H_6}$	$\frac{CH_3OH}{CH_4}$	$\frac{CH_3OH}{CO}$	$\frac{HCN}{NH_3}$	$\frac{HCN}{C_2H_6}$	$\frac{HCN}{CH_4}$	$\frac{HCN}{CO}$	$\frac{NH_3}{C_2H_6}$	$\frac{NH_3}{CH_4}$	$\frac{NH_3}{CO}$	$\frac{C_2H_6}{CH_4}$	$\frac{C_2H_6}{CO}$	$\frac{CH_4}{CO}$
$\frac{CH_3OH}{HCN}$	-	*0.36* *0.25* *10*	*0.55* *0.02* *16*	*0.23* *0.45* *11*	*0.05* *0.86* *12*	*-0.24* *0.44* *10*	*-0.75* *3x10^{-4}* *16*	*-0.58* *0.04* *11*	*-0.50* *0.06* *12*	-0.13 0.68 10	-0.25 0.52 7	0.18 0.63 7	0.08 0.79 11	-0.06 0.83 12	0.21 0.56 8
$\frac{CH_3OH}{NH_3}$	-	-	*-0.26* *0.40* *10*	*-0.08* *0.83* *7*	*0.50* *0.17* *7*	*0.80* *0.001* *10*	**-0.79** **0.002** **10**	-0.62 0.08 7	0.42 0.26 7	*-0.91* *4x10^{-5}* *10*	*-0.78* *0.01* *7*	*-0.30* *0.43* *7*	0.18 0.63 7	0.52 0.15 7	0.79 0.04 5
$\frac{CH_3OH}{C_2H_6}$	-	-	-	*0.58* *0.04* *11*	*-0.09* *0.75* *12*	-0.52 0.08 10	*0.06* *0.82* *16*	0.21 0.48 11	-0.38 0.18 12	*0.53* *0.07* *10*	0.58 0.10 7	0.23 0.55 7	*-0.15* *0.63* *11*	*-0.44* *0.12* *12*	-0.27 0.45 8
$\frac{CH_3OH}{CH_4}$	-	-	-	-	*0.88* *0.001* *8*	-0.48 0.19 7	0.20 0.50 11	*0.57* *0.04* *11*	0.78 0.007 8	0.37 0.33 7	*0.58* *0.10* *7*	0.75 0.05 5	*0.62* *0.02* *11*	0.67 0.03 8	*0.56* *0.09* *8*
$\frac{CH_3OH}{CO}$	-	-	-	-	-	0.25 0.52 7	-0.10 0.73 12	0.35 0.33 8	*0.78* *0.0008* *12*	-0.42 0.26 7	-0.36 -0.43 5	*0.65* *0.06* *7*	**0.70** **0.03** **8**	*0.90* *1x10^{-5}* *12*	*0.78* *0.008* *8*
$\frac{HCN}{NH_3}$	-	-	-	-	-	-	*-0.52* *0.08* *10*	*-0.62* *0.08* *7*	*0.33* *0.38* *7*	*-0.88* *1x10^{-4}* *10*	*-0.91* *5x10^{-4}* *7*	*-0.55* *0.12* *7*	-0.28 0.46 7	0.23 0.54 7	0.50 0.25 5
$\frac{HCN}{C_2H_6}$	-	-	-	-	-	-	-	*0.79* *4x10^{-4}* *13*	*0.29* *0.30* *13*	*0.82* *0.001* *10*	0.75 0.02 7	0.20 0.61 7	*-0.20* *0.48* *13*	*-0.19* *0.49* *13*	-0.39 0.23 9
$\frac{HCN}{CH_4}$	-	-	-	-	-	-	-	-	*0.41* *0.21* *9*	0.83 0.005 7	*0.83* *0.005* *7*	0.64 0.12 5	*0.38* *0.17* *13*	0.18 0.59 9	*-0.09* *0.79* *9*
$\frac{HCN}{CO}$	-	-	-	-	-	-	-	-	-	-0.37 0.33 7	-0.46 0.29 5	*0.53* *0.14* *7*	**0.75** **0.007** **9**	*0.80* *3x10^{-4}* *13*	*0.82* *0.002* *9*
$\frac{NH_3}{C_2H_6}$	-	-	-	-	-	-	-	-	-	-	*0.92* *5x10^{-4}* *7*	*0.48* *0.19* *7*	*N.A.*	*-0.50* *0.17* *7*	-0.71 0.07 5
$\frac{NH_3}{CH_4}$	-	-	-	-	-	-	-	-	-	-	-	*0.53* *0.22* *5*	*0.35* *0.36* *7*	-0.39 0.38 5	*-0.64* *0.12* *5*
$\frac{NH_3}{CO}$	-	-	-	-	-	-	-	-	-	-	-	-	0.61 0.15 5	*0.48* *0.19* *7*	*0.21* *0.64* *5*
$\frac{C_2H_6}{CH_4}$	-	-	-	-	-	-	-	-	-	-	-	-	-	*0.92* *7x10^{-5}* *9*	*0.56* *0.07* *9*
$\frac{C_2H_6}{CO}$	-	-	-	-	-	-	-	-	-	-	-	-	-	-	*0.77* *0.005* *9*
$\frac{CH_4}{CO}$	-	-	-	-	-	-	-	-	-	-	-	-	-	-	-

a) The ratios in the first raw and column are ratios between mixing ratios relative to water. For each cell, the first value represents the Spearman's correlation coefficient calculated excluding the upper limits; below each correlation coefficient, we report the (two-sided) level of significance (p) and the degrees of freedom (n) of the calculation (number of measures – 2); cells with good statistic ($p \leq 0.05$ and $n \geq 7$) are highlighted in green; correlations in bold numbers are shown in figures 9, and 10 and 11 and discussed in the text. Correlations between ratios that contain the same molecules in the numerator or denominator are reported in gray-italic.

Table 6: K and M factors for the studied comets.

	Comet	K[a]	M[a]	Group[b]
1	**07N3**	0.88	2.34	1
2	**99S4**	*0.05*	*0.18*	2
3	**99H1**	1.78	2.63	1
4	**09P1**	0.19	0.45	2
5	**12S1**	*0.54*	*0.43*	2
6	**12F6**	0.17	0.77	2
7	**99T1**	0.10	0.71	2
8	**00WM1**	2.21	1.44	3
9	**13R1**	0.20	0.66	2
10	**01A2**	2.04	0.88	3
11	**04Q2**	0.20	0.72	2
12	**07W1**	2.67	1.91	3
13	**8P**	*3.71*	*2.63*	3
14	**103P**	*8.10*	*7.21*	-
15	**73PB**	*0.95*	*0.64*	-
16	**73PC**	*0.70*	*1.06*	-
17	**17P**	*N.A.*	*N.A.*	*N.A.*
18	**10P**	*N.A.*	*N.A.*	*N.A.*
19	**9P**	*0.45*	*1.56*	-
20	**2P**	*2.12*	*1.67*	-

a) Italic indicates that the value was retrieved using at least an upper limit; b) groups are numbered following the description in section 3.2.2.

ONLINE MATERIAL: rotational temperatures, nucleus centered production rates and global production rates measured for the analyzed comets.

2P/Encke

Date	Setting	Molecule	T_{rot} [a] (K)	Q_{nc} [b] (x 10^{26} mol/s)	Q_{scale}	Q_{tot} (x 10^{26} mol/s)	MRs (% w.r.t. H_2O)
4-Nov-2003	KL1	CH_3OH	27 ± 3	0.62 ± 0.07	1.38 ± 0.16	0.85 ± 0.14	3.52 ± 0.50
		C_2H_6	(30)	0.08 ± 0.01		0.11 ± 0.02	0.46 ± 0.08
	KL2	H_2CO	(30)	< 0.013	1.38 ± 0.16	< 0.02	< 0.07
		CH_4	(30)	0.084 ± 0.007		0.12 ± 0.02	0.48 ± 0.06
		HCN	(30)	0.023 ± 0.005		0.032 ± 0.008	0.13 ± 0.03
		C_2H_2	(30)	< 0.015		< 0.02	< 0.08
		NH_3	(30)	< 0.14		< 0.19	< 0.8
	KL1 + KL2	H_2O	30 ± 2	17.5 ± 1.2	1.38 ± 0.16	24.2 ± 3.3	100
5-Nov-2003	KL1	CH_3OH	30 ± 2	0.92 ± 0.08	1.37 ± 0.10	1.26 ± 0.14	3.58 ± 0.33
		C_2H_6	(30)	0.15 ± 0.02		0.21 ± 0.03	0.58 ± 0.06
	MW	CO	(30)	< 0.52	1.37 ± 0.10	< 0.72	< 2.05
	KL1 + MW	H_2O	(30)	25.6 ± 1.0	1.37 ± 0.10	< 0.72	100
6-Nov-2003	KL2	H_2CO	(30)	< 0.02	1.74 ± 0.08	< 0.04	< 0.09
		CH_4	(30)	< 0.11		< 0.18	< 0.5
		HCN	(30)	0.014 ± 0.003		0.024 ± 0.006	0.07 ± 0.01
		C_2H_2	(30)	< 0.01		< 0.02	< 0.05
		NH_3	(30)	< 0.10		< 0.17	< 0.47
		H_2O	(30)	20.9 ± 1.1		36.4 ± 2.5	100
	MW	CO	(30)	< 0.40	1.74 ± 0.08	< 0.69	< 1.9
	KL2 + MW	H_2O	(30)	21.1 ± 1.1	1.74 ± 0.08	36.7 ± 2.6	100

a) Values in parenthesis are assumed; b) calculated for a common rotational temperature of 30 K for all the dates.

8P/Tuttle

Date	Setting	Molecule	T_{rot} [a] (K)	Q_{nc} [b] (x 10^{26} mol/s)	Q_{scale}	Q_{tot} (x 10^{26} mol/s)	MRs (% w.r.t. H_2O)
22-Dec-2007	KL1	CH_3OH	42 +2/-1	3.88 ± 0.17	1.43 ± 0.05	5.54 ± 0.31	2.61 ± 0.13
		C_2H_6	51 +18/-10	0.45 ± 0.04		0.65 ± 0.06	0.30 ± 0.03
		H_2O	50 ± 2	149 ± 4		205 ± 10	100

	KL2	H_2CO	(50)	0.16 ± 0.05	1.46 ± 0.10	0.23 ± 0.08	0.09 ± 0.03
		CH_4	(50)	0.46 ± 0.07		0.67 ± 0.12	0.27 ± 0.05
		HCN	39 ± 3	0.28 ± 0.04		0.41 ± 0.06	0.16 ± 0.03
		C_2H_2	(50)	< 0.08		< 0.12	< 0.05
		NH_3	(50)	< 0.89		< 1.30	< 0.51
		H_2O	50 ± 2	174 ± 13		253 ± 26	100
23-Dec-2007	KL2	H_2CO	(50)	0.15 ± 0.05	1.44 ± 0.07	0.22 ± 0.08	0.11 ± 0.04
		CH_4	(50)	0.36 ± 0.02		0.51 ± -.04	0.25 ± 0.02
		HCN	45 ± 5	0.22 ± 0.02		0.32 ± 0.03	0.15 ± 0.02
		C_2H_2	(50)	< 0.06		< 0.09	< 0.04
		NH_3	(50)	1.03 ± 0.54		1.49 ± 0.78	0.72 ± 0.38
		H_2O	52 ± 3	143 ± 10		206 ± 18	100
	MW	H_2O	(50)	100 ± 63	1.44 ± 0.07	172 ± 39	100
		CO	(50)	< 0.84		< 1.21	< 0.84

a) Values in parenthesis are assumed; b) calculated for a common rotational temperature of 50 K for all the dates.

10P/Tempel 2

Date	Setting	Molecule	T_{rot} [a] (K)	Q_{nc} [b] (x 10^{26} mol/s)	Q_{scale}	Q_{tot} (x 10^{26} mol/s)	MRs (% w.r.t. H_2O)
26-Jul-2010	KL1	CH_3OH	27 +3/-4	1.52 ± 0.17	1.54 ± 0.11	2.35 ± 0.32	1.81 ± 0.21
		C_2H_6	24 +9/-12	0.36 ± 0.03		0.55 ± 0.06	0.43 ± 0.04
	KL2	H_2CO	(35)	< 0.07	1.54 ± 0.11	< 0.17	< 0.09
		HCN	(35)	0.10 ± 0.02		0.16 ± 0.03	0.12 ± 0.02
		C_2H_2	(35)	< 0.06		< 0.13	< 0.06
		NH_3	(35)	0.94 ± 0.20		1.45 ± 0.33	1.12 ± 0.24
	KL1 + KL2	H_2O	35 ± 3	84 ± 3	1.54 ± 0.11	129 ± 10	100

a) Values in parenthesis are assumed; b) calculated for a common rotational temperature of 30 K for all the dates.

17P/Holmes

Date	Setting	Molecule	T_{rot} [a] (K)	Q_{nc} [b] (x 10^{26} mol/s)	Q_{scale}	Q_{tot} (x 10^{26} mol/s)	MRs (% w.r.t. H_2O)
27-Oct-2007	KL1	CH_3OH	70 +7/-6	97.4 ± 8.6	1.61 ± 0.07	157 ± 15	4.30 ± 0.43
		C_2H_6	(70)	52.4 ± 2.2		84 ± 5	2.31 ± 0.14
		H_2O	70 ± 4	2267 ± 106		3650 ± 233	100

30-Oct-2007	KL2	H_2CO	(70)	< 1.9	1.61 ± 0.07	< 3.1	< 0.16
		HCN	64 ± 2	7.07 ± 0.77		11.4 ± 1.33	0.61 ± 0.09
		C_2H_2	(70)	2.74 ± 1.18		4.41 ± 1.91	0.24 ± 0.11
		NH_3	(70)	18.6 ± 11.7		30 ± 19	0.82 ± 0.52
	MW	CO	(70)	102.2 ±28.8	1.61 ± 0.07	164 ± 47	8.8 ± 2.7
	KL2 + MW	H_2O	70 ± 3	1163 ± 125	1.61 ± 0.07	1720 ± 431	100

a) Values in parenthesis are assumed; b) calculated for a common rotational temperature of 70 K for all the dates.

9P/Tempel 1

Date	Setting	Molecule	T_{rot}[a] (K)	Q_{nc}[b] (x 10^{26} mol/s)	Q_{scale}	Q_{tot} (x 10^{26} mol/s)	MRs (% w.r.t. H_2O)
3-Jun-2005	KL1	CH_3OH	(27)	0.94 ± 0.32	1.53 ± 0.20	1.43 ± 0.53	3.1 ± 1.1
		C_2H_6	(27)	< 0.08		< 0.12	< 0.26
	KL2	HCN	(27)	0.07 ± 0.03	1.53 ± 0.20	0.11 ± 0.05	0.23 ± 0.10
	KL1 + KL2	H_2O	27 ± 3	31 ± 4	1.53 ± 0.20	47 ± 8	100
4-Jul-2005	KL1[c]	CH_3OH	(35)	0.75 ± 0.29	1.53 ± 0.20	1.14 ± 0.47	1.89 ± 0.91
		C_2H_6	(35)	0.09 ± 0.04		0.14 ± 0.07	0.23 ± 0.12
		H_2O	35 ± 3	40 ± 11		61 ± 19	100
	KL1[d]	CH_3OH	32 ± 8	2.47 ± 0.19	1.36 ± 0.07	3.36 ± 0.31	2.21 ± 0.20
		C_2H_6	37 ± 3	0.42 ± 0.05		0.58 ± 0.07	0.38 ± 0.05
		H_2O	35 ± 4	112 ± 5		146 ± 11	100
	KL2	H_2CO	(35)	0.20 ± 0.08	1.61 ± 0.12	0.32 ± 0.13	0.18 ± 0.07
		CH_4	(35)	0.74 ± 0.33		1.20 ± 0.55	0.66 ± 0.30
		HCN	29 +8/-6	0.27 ± 0.03		0.44 ± 0.06	0.24 ± 0.03
		C_2H_2	(35)	< 0.08		< 0.12	< 0.07
		NH_3	(35)	1.28 ± 0.80		2.05 ± 1.29	1.14 ± 0.72
		H_2O	35 ± 3	112 ± 5		190 ± 49	100
	MW	H_2O	(35)	118 ± 29	1.61 ± 0.12	154 ± 66	100
		CO	(35)	< 3.13		< 5.04	< 2.65
5-Jul-2005	MW	H_2O	(35)	52 ± 14	1.61 ± 0.12	82.8 ± 22.7	100
		CO	(35)	< 1.58		< 2.54	< 3.02

a) Values in parenthesis are assumed; b) calculated for a common rotational temperature of 27 K for the 3rd of June and 35 K for the 4th and 5th of July; c) pre-impact; d) post-impact

73P/Schwassman-Wachmann-B

Date	Setting	Molecule	T_{rot} [a] (K)	Q_{nc} [b] (x 10^{26} mol/s)	Q_{scale}	Q_{tot} (x 10^{26} mol/s)	MRs (% w.r.t. H_2O)
14-May-2006	KL1	CH_3OH	70 +8/-7	0.15 ± 0.02	1.81 ± 0.07	0.26 ± 0.04	0.37 ± 0.05
		C_2H_6	(100)	0.070 ± 0.004		0.126 ± 0.008	0.18 ± 0.01
		H_2O	92 ± 10	40 ± 1		79.5 ± 3.89	100
	KL2	H_2CO	(100)	0.016 ±0.003		0.029 ± 0.006	0.03 ± 0.01
		HCN	93 ± 2	0.132 ±0.004		0.24 ± 0.01	0.213 ± 0.009
		C_2H_2	(100)	0.019 ± 0.007		0.35 ± 0.01	0.03 ± 0.01
		NH_3	(100)	< 0.125		< 0.23	< 0.20
		H_2O	100 ± 5	62 ± 2		112 ± 54	100
15-May-2006	KL1	CH_3OH	(100)	0.16 ± 0.03	1.79 ± 0.05	0.28 ± 0.05	0.53 ± 0.09
		C_2H_6	(100)	0.067 ± 0.003		0.120 ± 0.007	0.23 ± 0.01
	KL2	H_2CO	(100)	0.013 ± 0.006		0.024 ± 0.010	0.04 ± 0.02
		HCN	78 +5/-4	0.110 ± 0.004		0.20 ± 0.01	0.38 ± 0.01
		C_2H_2	(100)	< 0.007		< 0.01	< 0.02
		NH_3	(100)	< 0.079		< 0.14	< 0.27
	KL1 + KL2	H_2O	100 ± 3	29.3 ± 0.3	1.79 ± 0.05	58.4 ± 2.7	100

a) Values in parenthesis are assumed; b) calculated for a common rotational temperature of 100 K for all the dates.

73P/Schwassman-Wachmann-C

Date	Setting	Molecule	T_{rot} [a] (K)	Q_{nc} [b] (x 10^{26} mol/s)	Q_{scale}	Q_{tot} (x 10^{26} mol/s)	MRs (% w.r.t. H_2O)
14-May-2006	KL1	CH_3OH	76 +12/-10	0.11 ± 0.02	1.84 ± 0.10	0.21 ± 0.03	0.49 ± 0.09
		C_2H_6	87 +11/-10	0.029 ± 0.001		0.053 ± 0.004	0.129 ± 0.005
	KL2	H_2CO	(85)	0.013 ± 0.004		0.025 ± 0.008	0.06 ± 0.02
		HCN	84 ± 2	0.077 ± 0.002		0.141 ± 0.008	0.343 ± 0.009
		C_2H_2	(85)	0.013 ± 0.004		0.024 ± 0.008	0.06 ± 0.02
		NH_3	(85)	< 0.077		< 0.14	< 0.34
	KL1 + KL2	H_2O	85 +3/-2	22.43 ± 0.45	1.84 ± 0.10	41.3 ± 2.4	100
15-May-2006	KL1	CH_3OH	(100)	0.26 ± 0.04	1.69 ± 0.06	0.44 ± 0.06	0.45 ± 0.07
		C_2H_6	(100)	0.090 ± 0.005		0.15 ± 0.01	0.155 ± 0.009
	KL2	H_2CO	(100)	0.029 ± 0.004	1.69 ± 0.06	0.048 ± 0.008	0.050 ± 0.007
		HCN	90 ± 4	0.160 ± 0.004		0.27 ± 0.01	0.276 ± 0.008

		C_2H_2	(100)	0.011 ± 0.006		0.018 ± 0.009	0.02 ± 0.01
		NH_3	(100)	< 0.086		< 0.15	< 0.15
	KL1 + KL2	H_2O	100 ± 2	58.0 ± 0.9	1.69 ± 0.06	98 ± 4	100

a) Values in parenthesis are assumed; b) calculated for a common rotational temperature of 85 K for the 14th of May and 100 for the 15th of May.

103P/Hartley 2

Date	Setting	Molecule	T_{rot} [a] (K)	Q_{nc} [b] (x 10^{26} mol/s)	Q_{scale}	Q_{tot} (x 10^{26} mol/s)	MRs (% w.r.t. H_2O)
16-Sep-2010	KL1	CH_3OH	(65)	0.56 ± 0.07	1.60 ± 0.20	0.89 ± 0.16	2.55 ± 0.41
		C_2H_6	66 +12/-9	0.171 ± 0.007		0.27 ± 0.04	0.78 ± 0.09
		H_2O	65 ± 3	21.9 ± 2.2		35.1 ± 5.6	100
	KL2	H_2CO	(65)	0.04 ± 0.02		0.07 ± 0.04	0.12 ± 0.06
		CH_4	(65)	< 0.27		< 0.43	< 0.8
		HCN	54 +10/-7	0.118 ± 0.009		0.19 ± 0.03	0.36 ± 0.06
		C_2H_2	(65)	0.04 ± 0.02		0.07 ± 0.03	0.12 ± 0.06
		NH_3	(65)	< 0.34		< 0.54	< 1.02
		H_2O	65 ± 3	33 ± 5		53 ± 10	100
18-Sep-2010	KL1	CH_3OH	39 ± 3	0.35 ± 0.08	(1.50)	0.52 ± 0.13	2.15 ± 0.56
		C_2H_6	66 +20/-14	0.13 ± 0.01		0.19 ± 0.02	0.80 ± 0.11
	KL2	H_2CO	(65)	< 0.03		< 0.04	< 0.16
		CH_4	(65)	< 0.24		< 0.36	< 1.5
		HCN	70 ± 15	0.05 ± 0.01		0.08 ± 0.02	0.30 ± 0.07
		C_2H_2	(65)	< 0.03		< 0.05	< 0.20
		NH_3	(65)	< 0.46		< 0.68	< 2.79
	KL1 + KL2	H_2O	65 ± 3	16 ± 2	(1.50)	29 ± 9	100
17-Oct-2010	KL1	CH_3OH	61 ± 3	0.95 ± 0.04	1.50 ± 0.05	1.42 ± 0.08	2.18 ± 0.10
		C_2H_6	75 +7/-2	0.34 ± 0.01		0.52 ± 0.03	0.78 ± 0.03
	KL2	H_2CO	(77)	< 0.018		< 0.02	< 0.03
		HCN	74 +8/-7	0.157 ± 0.006		0.24 ± 0.01	0.36 ± 0.01
		C_2H_2	(77)	0.057 ± 0.007		0.09 ± 0.01	0.13 ± 0.02
		NH_3	(77)	0.27 ± 0.10		0.41 ± 0.15	0.62 ± 0.23
	KL1 + KL2	H_2O	77 ± 3	43.5 ± 0.6	1.50 ± 0.05	65.3 ± 2.4	100
19-Oct-2010	KL1	CH_3OH	71 +4/-3	0.48 ± 0.03	1.76 ± 0.07	0.84 ± 0.06	2.14 ± 0.14
		C_2H_6	82 +10/-8	0.186 ± 0.008		0.33 ± 0.02	0.85 ± 0.05

	KL2	H_2CO	(77)	0.037 ± 0.008	1.76 ± 0.07	0.07 ± 0.02	0.18 ± 0.04
		HCN	68 +7/-6	0.051 ± 0.003		0.090 ± 0.06	0.22 ± 0.01
		C_2H_2	(77)	0.024 ± 0.008		0.04 ± 0.01	0.09 ± 0.04
		NH_3	(77)	< 0.14		< 0.25	< 0.65
	Kl1 + KL2	H_2O	77 ± 2	22.4 ± 0.4	1.76 ± 0.07	39.4 ± 1.7	100
21-Oct-2010	KL1[b]	CH_3OH	66 ± 3	1.30 ± 0.07	1.71 ± 0.04	2.21 ± 0.13	2.25 ± 0.13
		C_2H_6	89 +11/-9	0.49 ± 0.02		0.85 ± 0.03	0.85 ± 0.04
		H_2O	90 ± 2	57.9 ± 1.1		99 ± 3	100
	KL1[c]	CH_3OH	84 ± 5	0.85 ± 0.05	1.71 ± 0.04	1.45 ± 0.09	2.41 ± 0.15
		C_2H_6	84 +13/-10	0.25 ± 0.01		0.43 ± 0.02	0.71 ± 0.03
		H_2O	90 ± 2	35.3 ± 0.7		60.4 ± 1.9	100
	KL2	H_2CO	(90)	< 0.02	1.71 ± 0.04	< 0.03	< 0.03
		HCN	93 ± 3	0.091 ± 0.008		0.16 ± 0.02	0.18 ± 0.02
		C_2H_2	(90)	0.05 ± 0.02		0.08 ± 0.03	0.10 ± 0.02
		NH_3	(90)	0.33 ± 0.15		0.57 ± 0.26	0.67 ± 0.30
		H_2O	90 ± 2	49.5 ± 1.8		84.7 ± 3.6	100
22-Oct-2010	KL2	H_2CO	(80)	0.019 ± 0.009	1.65 ± 0.11	0.03 ± 0.02	0.05 ± 0.02
		HCN	73 +6/-5	0.110 ± 0.004		0.18 ± 0.02	0.29 ± 0.01
		C_2H_2	(80)	0.026 ± 0.006		0.04 ± 0.01	0.07 ± 0.02
		NH_3	(80)	0.21 ± 0.15		0.35 ± 0.25	0.56 ± 0.40
		H_2O	80 +4/-2	37.7 ± 1.3		62.3 ± 4.7	100
4-Nov-2010	KL1[d]	CH_3OH	67 +6/-5	1.38 ± 0.09	1.49 ± 0.04	2.06 ± 0.14	2.73 ± 0.22
		C_2H_6	84 +11/-9	0.45 ± 0.02		0.67 ± 0.03	0.89 ± 0.05
		H_2O	74 ± 3	50.5 ± 2.5		75.3 ± 4.3	100
	KL1[e]	CH_3OH	66 ± 6	1.91 ± 0.07	1.49 ± 0.04	2.84 ± 0.12	2.46 ± 0.10
		C_2H_6	81 +7/-5	1.01 ± 0.02		1.50 ± 0.05	1.30 ± 0.04
		H_2O	74 ± 3	77.7 ± 1.5		116 ± 4	100
	KL2	H_2CO	(74)	< 0.01	1.56 ± 0.04	< 0.02	< 0.02
		HCN	72 +8/-7	0.19 ± 0.01		0.30 ± 0.02	0.29 ± 0.02
		C_2H_2	(74)	0.076 ± 0.008		0.12 ± 0.01	0.12 ± 0.01
		H_2O	74 ± 3	64.7 ± 2.5		101 ± 4.6	100
		NH_3	74	0.54 ± 0.09		0.84 ± 0.14	0.83 ± 0.14
16-Nov-2010	KL2	H_2CO	(67)	< 0.05	1.67 ± 0.16	<0.09	< 0.06
		HCN	(67)	0.17 ± 0.02		0.28 ± 0.04	0.19 ± 0.03
		C_2H_2	(67)	< 0.04		< 0.07	< 0.05

	NH_3	(67)	0.51 ± 0.04		0.85 ± 0.11	0.58 ± 0.08
	H_2O	67 ± 5	87.8 ± 9.4		147 ± 21	100

a) Values in parenthesis are assumed; b) calculated for a common rotational temperature of 65 K for the 16th and 18th of September, 77 K for the 17th and 19th of October, 90 K for the 21st of October, 80 K for the 22nd of October, 74 K for the 4th of November, 67 K for the 16th of November; c) UT 11:00; d) UT 15:30; e) UT 11:00; f) UT 15:30.

C/1999 H1 (Lee)

Date	Setting	Molecule	T_{rot} [a] (K)	Q_{nc} [b] (x 10^{26} mol/s)	Q_{scale}	Q_{tot} (x 10^{26} mol/s)	MRs (% w.r.t. H_2O)
19-Aug-1999	MW	H_2O	(70)	675 ± 84	2.06 ± 0.20	1390 ± 220	100
		CO	(70)	10 ± 2		20.6 ± 4.9	1.48 ± 0.37
20-Aug-1999	KL1	CH_3OH	59 ± 3	21.7 ± 0.9	1.52 ± 0.04	33.0 ± 1.6	3.20 ± 0.16
		C_2H_6	68 +7/-6	6.0 ± 0.2		9.12 ± 0.39	0.89 ± 0.04
	KL2	H_2CO	(70)	1.6 ± 0.3	1.52 ± 0.04	2.45 ± 0.45	0.24 ± 0.04
		CH_4	(70)	7.3 ± 0.6		11.1 ± 0.9	1.07 ± 0.09
		HCN	61 +11/8	1.26 ± 0.10		1.91 ± 0.16	0.19 ± 0.02
		C_2H_2	(70)	0.59 ± 0.15		0.89 ± 0.24	0.09 ± 0.04
		NH_3	(70)	3.82 ±1.01		5.81 ± 1.54	0.56 ± 0.15
	KL1 + KL2	H_2O	70 ± 2	678 ± 18	1.52 ± 0.04	1030 ± 39	100

a) Values in parenthesis are assumed; b) calculated for a common rotational temperature of 70 K for all the dates.

C/1999 S4 (LINEAR)

Date	Setting	Molecule	T_{rot} [a] (K)	Q_{nc} [b] (x 10^{26} mol/s)	Q_{scale}	Q_{tot} (x 10^{26} mol/s)	MRs (% w.r.t. H_2O)
13-Jul-2000	KL1	CH_3OH	(75)	< 0.94	1.47 ± 0.03	< 1.38	< 0.13
		C_2H_6	(75)	0.55 ± 0.11		0.81 ± 0.16	0.11 ± 0.02
		CH_4	(75)	1.00 ± 0.37		1.47 ± 0.55	0.20 ± 0.08
		H_2O	75 ± 5	500 ± 32		735 ± 50	100
	KL2	H_2CO	(75)	< 0.32	1.47 ± 0.03	< 0.47	< 0.06
		CH_4	(75)	0.76 ± 0.28		1.12 ± 0.04	0.23 ± 0.08
		HCN	(75)	0.14 ± 0.04		0.20 ± 0.08	0.04 ± 0.01
		C_2H_2	(75)	< 0.23		< 0.36	< 0.05
		NH_3	(75)	< 3.84		< 5.64	< 0.76
		H_2O	(75)	337 ± 26		495 ± 40	100

	MW	H_2O	(75)	204 ± 45	1.47 ± 0.03	303 ± 56	100
		CO	(75)	2.78 ± 0.89		4.11 ± 0.89	1.36 ± 0.53

a) Values in parenthesis are assumed; b) calculated for a common rotational temperature of 75 K for all the dates.

C/1999 T1 (McNaught-Hartley)

Date	Setting	Molecule	T_{rot} [a] (K)	Q_{nc} [b] (x 10^{26} mol/s)	Q_{scale}	Q_{tot} (x 10^{26} mol/s)	MRs (% w.r.t. H_2O)
14-Jan-2001	KL1	CH_3OH	57 +4/-3	18.1 ± 1.2	1.52 ± 0.05	27.6 ± 2.0	4.22 ± 0.69
		C_2H_6	65 +13/-9	4.67 ± 0.21		7.10 ± 0.39	1.09 ± 0.17
	KL2	H_2CO	(60)	< 0.88	1.52 ± 0.05	< 1.34	< 0.20
		HCN	(60)	2.05 ± 0.93		3.11 ± 1.42	0.48 ± 0.23
		C_2H_2	(60)	< 1.18		< 1.79	< 0.27
		NH_3	(60)	< 18.21		< 27.7	< 4.2
	MW-1	CO	(60)	50 ± 10	1.52 ± 0.05	76 ± 15	11.5 ± 2.8
	KL1 + KL2	CH_4	(60)	11.7 ± 6.8	1.52 ± 0.05	17.8 ± 10.3	2.73 ± 1.63
	KL1 + KL2 + MW	H_2O	60 ± 4	430 ± 65	1.52 ± 0.05	654 ± 100	100
5-Feb-2001	KL1	CH_3OH	49 ± 3	9.85 ± 0.84	1.54 ± 0.22	15.2 ± 2.5	3.41 ± 0.45
		C_2H_6	41 ± 5	2.87 ± 0.33		4.43 ± 0.81	0.99 ± 0.15
	KL2	H_2CO	(52)	0.40 ± 0.13	1.54 ± 0.22	0.62 ± 0.22	0.14 ± 0.05
		HCN	56 ± 8	0.42 ± 0.06		0.65 ± 0.13	0.15 ± 0.03
		C_2H_2	(52)	0.80 ± 0.18		1.23 ± 0.32	0.27 ± 0.07
		NH_3	(52)	< 3.18		< 4.89	< 1.1
		H_2O	52 +7/-8	289 ± 29		445 ± 78	100
6-Feb-2001	MW	H_2O	(52)	308 ± 50	1.54 ± 0.22	474 ± 103	100
		CO	(52)	73 ± 16		112 ± 30	23.7 ± 6.5

a) Values in parenthesis are assumed; b) calculated for a common rotational temperature of 60 K for the 14th of January and 52 K for the 5th and 6th of February.

C/2000 WM_1 (LINEAR)

Date	Setting	Molecule	T_{rot} [a] (K)	Q_{nc} [b] (x 10^{26} mol/s)	Q_{scale}	Q_{tot} (x 10^{26} mol/s)	MRs (% w.r.t. H_2O)
23-Nov-2001	KL1	CH_3OH	56 ± 3	3.37 ± 0.18	1.54 ± 0.04	5.18 ± 0.30	1.78 ± 0.21
		C_2H_6	61 +6/-5	1.12 ± 0.04		1.73 ± 0.08	0.59 ± 0.07
		H_2O	70 ± 3	189 ± 20		291 ± 32	100

		H_2CO	(70)	< 0.07		< 0.11	< 0.03
		CH_4	(70)	0.78 ± 0.09		1.19 ± 0.15	0.33 ± 0.04
	KL2	HCN	69 +8/-6	0.45 ± 0.04	1.54 ± 0.04	0.69 ± 0.07	0.19 ± 0.02
		C_2H_2	(70)	0.14 ± 0.08		0.22 ± 0.01	0.06 ± 0.03
		NH_3	(70)	< 1.01		< 1.55	< 0.42
		H_2O	70 ± 3	239 ± 14		368 ± 24	100
24-Nov-2001	KL1	CH_3OH	54 +4/-3	2.03 ± 0.16	1.62 ± 0.05	3.30 ± 0.27	1.12 ± 0.10
		C_2H_6	69 +8/-7	0.89 ± 0.03		1.44 ± 0.07	0.49 ± 0.02
	KL2	H_2CO	(78)	0.12 ± 0.05	1.62 ± 0.05	0.20 ± 0.08	0.07 ± 0.03
		CH_4	(78)	0.87 ± 0.07		1.41 ± 0.13	0.48 ± 0.04
		HCN	72 ± 5	0.40 ± 0.03		0.65 ± 0.06	0.22 ± 0.02
		C_2H_2	(78)	0.12± 0.07		0.20 ± 0.11	0.07 ± 0.04
		NH_3	(78)	< 0.96		< 1.55	< 0.52
	KL1 + KL2	H_2O	78 ± 5	182 ± 6	1.62 ± 0.05	294 ± 14	100
	MW	CO	78	2.09 ± 0.87	1.62 ± 0.05	3.39 ± 1.42	0.69 ± 0.30
		H_2O	78	305 ± 32		494 ± 54	100

a) Values in parenthesis are assumed; b) calculated for a common rotational temperature of 70 K for the 23rd of November and 78 K for the 24th of November.

C/2001 A2 (LINEAR)

Date	Setting	Molecule	T_{rot}[a] (K)	Q_{nc}[b] (x 10^{26} mol/s)	Q_{scale}	Q_{tot} (x 10^{26} mol/s)	MRs (% w.r.t. H_2O)
9-Jul-2001	KL1	CH_3OH	82 ± 4	9.27 ± 0.31	1.60 ± 0.03	14.5 ± 0.56	5.1 ± 0.6
		C_2H_6	86 ± 5	5.84 ± 0.10		9.11 ± 0.24	3.20 ± 0.34
	KL2	H_2CO	(85)	0.14 ± 0.05	1.60 ± 0.03	0.23 ± 0.08	0.08 ± 0.03
		CH_4	(85)	2.86 ± 0.45		4.74 ± 0.75	1.67 ± 0.31
		HCN	66 +7/-8	0.52 ±0.05		0.86 ± 0.09	0.30 ± 0.04
		C_2H_2	(85)	0.25 ±0.07		0.41 ± 0.11	0.14 ± 0.04
		NH_3	(85)	< 1.03		< 1.73	< 0.61
	KL1 + KL2	H_2O	85 ± 5	189 ± 19	1.60 ± 0.03	284 ± 29	100
10-Jul-2001	KL1	CH_3OH	82 +5/-6	7.19 ± 0.28	1.50 ± 0.03	10.6 ± 0.5	3.8 ± 0.3
		C_2H_6	82 ± 4	4.84 ± 0.11		7.16 ± 0.25	2.57 ± 0.19
	KL2	H_2CO	(85)	< 0.08	1.50 ± 0.03	< 0.11	< 0.04
		CH_4	(85)	3.38 ± 0.28		5.10 ± 0.44	1.83 ± 0.20
		HCN	67 +5/-4	0.55 ± 0.03		0.84 ± 0.05	0.31 ± 0.04

		C_2H_2	(85)	0.25 ± 0.04		0.38 ± 0.06	0.14 ± 0.02
		NH_3	(85)	< 0.95		< 1.42	< 0.51
	KL1 + KL2	H_2O	85 ± 5	185 ± 12	1.50 ± 0.03	278 ± 18	100
	MW	H_2O	(85)	194.4 ± 50.7	1.50 ± 0.03	293 ± 77	100
		CO	(85)	6.00 ± 0.6		9.0 ± 2.0	3.07 ± 0.96

a) Values in parenthesis are assumed; b) calculated for a common rotational temperature of 85 K for all the dates.

C/2004 Q2 (Machholz)

Date	Setting	Molecule	T_{rot}[a] (K)	Q_{nc}[b] (x 10^{26} mol/s)	Q_{scale}	Q_{tot} (x 10^{26} mol/s)	MRs (% w.r.t. H_2O)
28-Nov-2004	KL1	CH_3OH	61 +3/-4	18.88 ± 1.24	1.52 ± 0.05	28.7 ± 2.1	4.08 ± 0.39
		C_2H_6	91 +16/-12	6.33 ± 0.29		9.62 ± 0.54	1.37 ± 0.11
	KL2	H_2CO	(85)	0.50 ± 0.22	1.52 ± 0.05	0.75 ± 0.34	0.11 ± 0.05
		CH_4	(85)	8.29 ± 0.45		12.6 ± 0.80	1.79 ± 0.16
		HCN	94 +6/-5	1.51 ± 0.14		2.30 ± 0.23	0.33 ± 0.04
		C_2H_2	(85)	0.62 ± 0.29		0.94 ± 0.44	0.13 ± 0.06
		NH_3	(85)	< 6.03		< 9.16	< 1.3
	KL1 + KL2	H_2O	85 ± 4	463 ± 32	1.52 ± 0.05	704 ± 54	100
	MW	H_2O	(85)	490 ± 45	1.52 ± 0.05	745 ± 73	100
		CO	79 ± 6	23.66 ± 2.39		36 ± 4	4.83 ± 0.66
19-Jan-2005	KL1	CH_3OH	71 +2/-1	27.9 ± 0.6	1.53 ± 0.02	42.6 ± 1.0	1.77 ± 0.06
		C_2H_6	90 +12/-10	10.30 ± 0.32		15.8 ± 0.53	0.65 ± 0.03
		H_2O	80 ± 4	1578 ± 42		2410 ± 71	100
	KL2	H_2CO	(80)	1.05 ± 0.12	1.64 ± 0.04	1.72 ± 0.20	0.061 ± 0.008
		CH_4	(80)	21.07 ± 0.62		34.6 ± 1.3	1.23 ± 0.07
		HCN	89 +5/-4	2.53 ± 0.09		4.16 ± 0.18	0.15 ± 0.01
		C_2H_2	(80)	1.15 ± 0.14		1.89 ± 0.24	0.067 ± 0.009
		NH_3	(80)	4.12 ± 0.12		6.75 ± 0.25	0.24 ± 0.01
		H_2O	(80)	1713 ± 84		2810 ± 154	100

a) Values in parenthesis are assumed; b) calculated for a common rotational temperature of 85 K for the 28th of November and 80 K for the 19th of January.

C/2007 N3 (Lulin)

Date	Setting	Molecule	T_{rot}[a] (K)	Q_{nc}[b] (x 10^{26} mol/s)	Q_{scale}	Q_{tot} (x 10^{26} mol/s)	MRs (% w.r.t. H_2O)
31-Jan-2009	KL2	H_2CO	(68)	0.81 ± 0.13	1.64 ± 0.06	1.33 ± 0.21	0.15 ± 0.02
		CH_4	59 +4/-5	7.20 ± 0.26		11.8 ± 0.6	1.29 ± 0.06
		HCN	67 +7/-6	0.77 ± 0.07		1.27 ± 0.12	0.14 ± 0.01
		C_2H_2	(68)	0.46 ± 0.09		0.76 ± 0.15	0.08 ± 0.02
		NH_3	(68)	< 1.54		< 2.53	< 0.28
		H_2O	68 ± 4	556 ± 19		912 ± 46	100
1-Feb-2009	KL1	CH_3OH	57 ± 3	34.59 ± 1.18	1.48 ± 0.01	51.2 ± 1.78	3.82 ± 0.15
		C_2H_6	77 +13/-10	7.20 ± 0.30		10.7 ± 0.44	0.80 ± 0.04
		H_2O	65 ± 1	906 ± 16		1340 ± 25	100
		NH_3	(65)	2.44 ± 1.41		3.62 ± 2.06	0.27 ± 0.16
	MW	H_2O	63 ± 2	1427 ± 27	1.64 ± 0.11	2340 ± 163	100
		CO	77 ± 11	37.8 ± 2.0		62.3 ± 5.3	2.66 ± 0.15

a) Values in parenthesis are assumed; b) calculated for a common rotational temperature of 68 K for the 31st of January, 65 K for the 1st of February KL1 setting, 63 K for the 1st of February MW setting.

C/2007 W1 (Boattini)

Date	Setting	Molecule	T_{rot}[a] (K)	Q_{nc}[b] (x 10^{26} mol/s)	Q_{scale}	Q_{tot} (x 10^{26} mol/s)	MRs (% w.r.t. H_2O)
9-Jul-2008	KL1	CH_3OH	83 +5/-4	3.38 ± 0.12	3.48 ± 0.10	11.7 ± 0.5	4.28 ± 0.22
		C_2H_6	80 ± 3	1.58 ± 0.04	1.63 ± 0.10	2.58 ± 0.17	0.92 ± 0.07
	KL2	H_2CO	(83)	< 0.03	1.63 ± 0.10	< 0.05	< 0.02
		HCN	84 +7/-6	0.38 ± 0.01		0.61 ± 0.04	0.22 ± 0.02
		C_2H_2	(83)	0.21 ± 0.02		0.34 ± 0.04	0.13 ± 0.02
		NH_3	(83)	1.27 ± 0.20		2.07 ± 0.36	0.76 ± 0.14
	KL1 + KL2	CH_4	(83)	1.41 ± 0.20	1.63 ± 0.10	2.30 ± 0.34	0.78 ± 0.15
		H_2O	83 ± 4	78 ± 2	3.48 ± 0.10	272 ± 11	100
10-Jul-2008	KL1	CH_3OH	83 +5/-4	2.92 ± 0.08	3.48 ± 0.10	10.4 ± 0.4	3.93 ± 0.25
		C_2H_6	78 +5/-4	1.44 ± 0.03	1.63 ± 0.10	2.59 ± 0.15	0.92 ± 0.07
	MW	CO	(83)	2.86 ± 0.36	1.63 ± 0.10	4.84 ± 0.7	1.83 ± 0.31
	KL1 + MW	H_2O	(83)	76 ± 5	3.48 ± 0.10	264 ± 20	100

a) Values in parenthesis are assumed; b) calculated for a common rotational temperature of 83 K for all the dates.

C/2009 P1 (Garrad)

Date	Setting	Molecule	T_{rot}[a] (K)	Q_{nc}[b] (x 10^{26} mol/s)	Q_{scale}	Q_{tot} (x 10^{26} mol/s)	MRs (% w.r.t. H_2O)
13-Oct-2011	KL1	CH_3OH	52 +5/-4	15.3 ± 2.6	1.42 ± 0.15	21.8 ± 4.4	2.13 ± 0.46
		C_2H_6	46 +8/-6	4.76 ± 0.27		6.76 ± 0.81	0.66 ± 0.09
		H_2O	50 ± 2	719 ± 92		1020 ± 170	100
	KL2	H_2CO	(50)	< 0.31	1.64 ± 0.08	< 0.5	< 0.07
		CH_4	(50)	5.57 ± 0.28		9.14 ± 0.64	1.22 ± 0.11
		HCN	71 +10/-8	1.50 ± 0.09		2.45 ± 0.19	0.33 ± 0.03
		C_2H_2	(50)	< 0.31		< 0.5	< 0.07
		NH_3	(50)	4.69 ± 3.68		7.69 ± 6.05	1.03 ± 0.81
		H_2O	50 ± 2	456 ± 33		747 ± 65	100
	MW	H_2O	(50)	(456 ± 33)[c]	1.86 ± 0.16	847 ± 95	100
		CO	(50)	35.13 ± 9.38		65.3 ± 18.3	7.71 ± 2.13
9-Jan-2012	KL1	CH_3OH	46 ± 5	11.1 ± 0.8	1.70 ± 0.07	18.9 ± 1.6	2.96 ± 0.52
		C_2H_6	60 +6/-7	3.76 ± 0.16		6.39 ± 0.37	1.00 ± 0.17
	KL2	H_2CO	(60)	< 0.25	1.79 ± 0.11	< 0.44	< 0.07
		CH_4	(60)	6.90 ± 0.56		12.3 ± 1.3	1.84 ± 0.33
		HCN	(60)	1.36 ± 0.12		2.44 ± 0.26	0.36 ± 0.07
		C_2H_2	(60)	0.67 ± 0.23		1.19 ± 0.42	0.18 ± 0.07
		NH_3	(60)	< 2.65		< 4.74	< 0.71
	KL1 + KL2	H_2O	60 ± 2	375 ± 60		671 ± 115	100
10-Jan-2012	KL1	CH_3OH	43 +4/-3	9.7 ± 0.6	1.69 ± 0.11	16.4 ± 1.5	2.21 ± 0.21
		C_2H_6	57 +5/-4	2.77 ± 0.14		4.68 ± 0.39	0.63 ± 0.05
		H_2O	60 ± 2	740 ± 31		743 ± 71	1250 ± 97
	KL2	H_2CO	(60)	< 0.34	1.85 ± 0.09	< 0.62	< 0.05
		CH_4	(60)	5.09 ± 0.59		9.41 ± 1.19	0.76 ± 0.10
		HCN	57 ± 3	1.14 ± 0.14		2.10 ± 0.27	0.17 ± 0.02
		C_2H_2	(60)	1.00 ± 0.28		1.85 ± 0.53	0.15 ± 0.04
		NH_3	(60)	< 2.94		< 5.43	< 0.44
		H_2O	60 ± 2	674 ± 48		1250 ± 107	1247 ± 108

a) Values in parenthesis are assumed; b) calculated for a common rotational temperature of 50 K for the 13th of October, 60 K for the 9th and 10th of January. the dates; c) assumed.

C/2012 F6 (Lemmon)

Date	Setting	Molecule	T_{rot}[a] (K)	Q_{nc}[b] (x 10^{26} mol/s)	Q_{scale}	Q_{tot} (x 10^{26} mol/s)	MRs (% w.r.t. H_2O)
20-Jun-2013	KL1	CH_3OH	45 +11/-8	10.36 ± 1.02	1.63 ± 0.06	16.9 ± 1.78	1.46 ± 0.20
		C_2H_6	50 ± 3	2.23 ± 0.21		3.63 ± 0.36	0.31 ± 0.04
	KL2	H_2CO	(53)	< 0.33	1.63 ± 0.06	< 0.54	< 0.05
		HCN	41 +10/-7	1.37 ± 0.21		2.24 ± 0.36	0.19 ± 0.04
		C_2H_2	(53)	< 0.38		< 0.62	< 0.05
		NH_3	(53)	4.10 ± 1.61		6.69 ± 2.64	0.58 ± 0.23
	KL1 + KL2	H_2O	53 ± 3	441 ± 29	2.63 ± 0.14	1160 ± 97	100

a) Values in parenthesis are assumed; b) calculated for a common rotational temperature of 53 K.

C/2012 S1 (LINEAR)

Date	Setting	Molecule	T_{rot}[a] (K)	Q_{nc}[b] (x 10^{26} mol/s)	Q_{scale}	Q_{tot} (x 10^{26} mol/s)	MRs (% w.r.t. H_2O)
22-Oct-2013	KL1	CH_3OH	(50)	< 0.84	1.72 ± 0.12	< 1.45	< 1.66
		C_2H_6	(50)	0.27 ± 0.07		0.47 ± 0.13	0.54 ± 0.19
		H_2O	(50)	50± 12		86 ± 21	100
24-Oct-2013	KL1	CH_3OH	(50)	< 0.57	1.61 ± 0.10	< 0.91	< 1.21
		C_2H_6	(50)	0.20 ± 0.06		0.32 ± 0.01	0.43 ± 0.13
		H_2O	(50)	47 ± 2		76 ± 6	100
	MW	H_2O	(50)	135 ± 46	1.61 ± 0.10	217 ± 75	100
		CO	(50)	< 3.41		< 5.48	< 2.52
25-Oct-2013	KL2	H_2CO	(53)	< 0.11	1.42 ± 0.22	< 0.16	< 0.24
		CH_4	(53)	< 0.09		< 0.12	< 0.18
		HCN	(53)	< 0.07		< 0.09	< 0.14
		C_2H_2	(53)	< 0.12		< 0.17	< 0.26
		NH_3	(53)	< 1.19		< 1.69	< 2.54
		H_2O	53 ± 5	47 ± 13		67 ± 21	100
7-Nov-2013	KL2	H_2CO	(63)	< 0.24	1.98 ± 0.30	< 0.48	< 0.10
		CH_4	(63)	0.92 ± 0.12		1.82 ± 0.36	0.41 ± 0.06
		HCN	(63)	0.21 ± 0.05		0.42 ± 0.12	0.09 ± 0.02
		C_2H_2	(63)	0.22 ± 0.11		0.44 ± 0.23	0.10 ± 0.05
		NH_3	(63)	< 1.52		< 3.01	< 0.68
		H_2O	63 ± 4	222 ± 19		439 ± 76	100

a) Values in parenthesis are assumed; b) calculated for a common rotational temperature of 50 K for the 22nd and 24th of October, 53 K for the 25th of October and 63 K for the 7th of November.

C/2013 R1 (Lovejoy)

Date	Setting	Molecule	T_{rot}[a] (K)	Q_{nc}[b] (x 10^{26} mol/s)	Q_{scale}	Q_{tot} (x 10^{26} mol/s)	MRs (% w.r.t. H_2O)
22-Oct-2013	KL1	CH_3OH	57 +8/-7	3.82 ± 0.28	1.60 ± 0.09	6.11 ± 0.57	4.77 ± 0.42
		C_2H_6	62 +15/-10	0.91 ± 0.06		1.45 ± 0.13	1.14 ± 0.09
	KL2	H_2CO	(58)	< 0.38	1.60 ± 0.09	< 0.23	< 0.19
		CH_4	(58)	0.85 ± 0.06		1.35 ± 0.12	1.06 ± 0.09
		HCN	70 ± 16	0.18 ± 0.07		0.30 ± 0.12	0.23 ± 0.09
		C_2H_2	(58)	< 0.14		< 0.23	< 0.17
		NH_3	(58)	< 1.85		< 2.96	< 2.31
	KL1 + KL2	H_2O	58 ± 4	80 ± 4	1.60 ± 0.09	128 ± 10	100
24-Oct-2013	MW	H_2O	(58)	80 ± 27	1.60 ± 0.09	128 ± 45	100
		CO	(58)	7.48 ± 0.35		12.0 ± 0.88	9.32 ± 3.22
25-Oct-2013	KL2	H_2CO	(60)	< 0.12	1.63 ± 0.12	< 0.19	< 0.05
		CH_4	(60)	2.72 ± 0.08		4.44 ± 0.35	1.11 ± 0.07
		HCN	61 ± 3	0.66 ± 0.06		1.08 ± 0.13	0.27 ± 0.03
		C_2H_2	(60)	0.20 ± 0.06		0.32 ± 0.10	0.08 ± 0.02
		NH_3	(60)	4.58 ± 1.38		7.47 ± 2.32	1.87 ± 0.57
		H_2O	60 ± 2	245.63 ± 13.23		400 ± 37	100
27-Oct-2013	KL1	CH_3OH	55 +7/-6	5.06 ± 0.35	1.50 ± 0.08	7.60 ± 0.66	2.35 ± 0.23
		C_2H_6	58 ± 3	1.10 ± 0.07		1.65 ± 0.14	0.51 ± 0.05
		H_2O	60 ± 2	215 ± 15		323 ± 28	100
	KL2	H_2CO	(60)	< 0.15	1.50 ± 0.08	< 0.22	< 0.15
		CH_4	(60)	1.29 ± 0.02		1.94 ± 0.11	1.30 ± 0.15
		HCN	50 ± 5	0.22 ± 0.06		0.34 ± 0.10	0.22 ± 0.07
		C_2H_2	(60)	< 0.11		< 0.17	< 0.11
		NH_3	(60)	< 1.52		< 2.29	< 1.54
		H_2O	60 ± 2	99 ± 11		149 ± 19	100
28-Oct-2013	KL2	H_2CO	(65)	< 0.13	1.30 ± 0.07	< 0.17	< 0.04
		CH_4	(65)	4.24 ± 0.29		5.51 ± 0.48	1.31 ± 0.11
		HCN	62 +9/-7	0.72 ± 0.04		0.94 ± 0.08	0.22 ± 0.02
		C_2H_2	(65)	0.29 ± 0.06		0.38 ± 0.08	0.09 ± 0.02

		NH_3	(65)	4.92 ± 1.35		6.40 ± 1.79	1.52 ± 0.42
		H_2O	65 ± 2	324 ± 14		421 ± 29	100
29-Oct-2013	KL2	H_2CO	(65)	< 0.14	1.67 ± 0.16	< 0.24	< 0.08
		CH_4	(65)	1.84 ± 0.11		3.08 ± 0.35	1.03 ± 0.08
		HCN	70 ± 8	0.49 ± 0.06		0.81 ± 0.13	0.27 ± 0.04
		C_2H_2	(65)	< 0.13		< 0.22	< 0.07
		NH_3	(65)	< 1.89		< 3.16	< 1.06
	MW	CO	56 +8/-7	14.24 ± 0.53		22.8 ± 1.31	7.94 ± 0.51
	MW + KL2	H_2O	65 ± 3	179 ± 9		299 ± 32	100
7-Nov-2013	KL2	H_2CO	(73)	0.21 ± 0.05	1.56 ± 0.05	0.32 ± 0.08	0.08 ± 0.02
		CH_4	(73)	3.55 ± 0.19		5.54 ± 0.34	1.38 ± 0.08
		HCN	69 ± 3	0.68 ± 0.05		1.07 ± 0.08	0.26 ± 0.02
		C_2H_2	(73)	0.18 ± 0.09		0.28 ± 0.13	0.07 ± 0.03
		NH_3	(73)	2.95 ± 1.25		4.61 ± 1.96	1.14 ± 0.49
		H_2O	73 ± 2	258 ± 8		402 ± 18	100

a) Values in parenthesis are assumed; b) calculated for a common rotational temperature of 58 K for the 22nd and 24th of October, 60 K for the 25th and 27th of October and 65 K for the 28th and 29th of October and 73 K for the 7th of November.